THIS REPORT HAS BEEN DELIMITED
AND CLEARED FOR PUBLIC RELEASE
UNDER DOD DIRECTIVE 5200.20 AND
NO RESTRICTIONS ARE IMPOSED UPON
ITS USE AND DISCLOSURE.

DISTRIBUTION STATEMENT A

APPROVED FOR PUBLIC RELEASE;
DISTRIBUTION UNLIMITED.

DISCLAIMER NOTICE

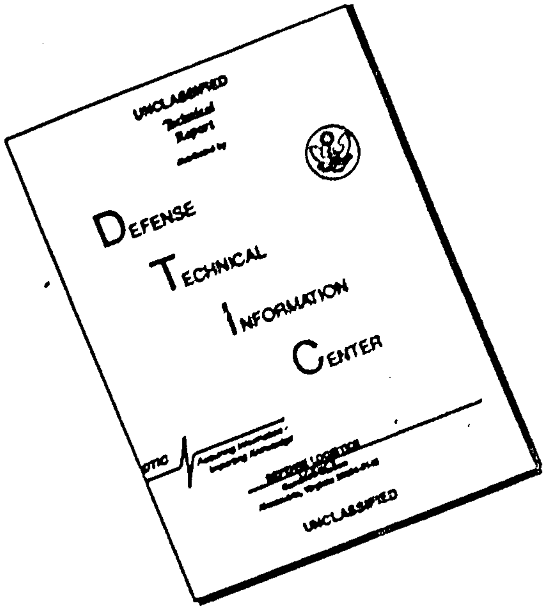

THIS DOCUMENT IS BEST QUALITY AVAILABLE. THE COPY FURNISHED TO DTIC CONTAINED A SIGNIFICANT NUMBER OF PAGES WHICH DO NOT REPRODUCE LEGIBLY.

CONFIDENTIAL

AD No. 126610

ASTIA FILE COPY

BRL

OCC075

REPORT No. 994

SEPTEMBER 1956

FC

The Magnus Characteristics Of A 30-MM Aircraft Bullet (U)

A. S. PLATOU

J. STERNBERG

957

57A 14311

DEPARTMENT OF THE ARMY PROJECT No. 5B0307002

ORDNANCE RESEARCH AND DEVELOPMENT PROJECT No. TB3-0426

BALLISTIC RESEARCH LABORATORIES

ABERDEEN PROVING GROUND, MARYLAND

CONFIDENTIAL

CONFIDENTIAL

B A L L I S T I C   R E S E A R C H   L A B O R A T O R I E S

REPORT NO. 994

SEPTEMBER 1956

THE MAGNUS CHARACTERISTICS OF A 30 MM AIRCRAFT BULLET (U)

A. S. Platou

J. Sternberg

Department of the Army Project No. 5B0307002
Ordnance Research and Development Project No. TB3-0426

A B E R D E E N   P R O V I N G   G R O U N D,   M A R Y L A N D

CONFIDENTIAL

TABLE OF CONTENTS

ACKNOWLEDGMENT

The authors wish to acknowledge the important contributions of other members of the wind tunnel group in carrying out this program. We particularly wish to mention the aid received from the Instrumentation Section, headed by Dr. T. L. Smith, in developing the air turbine, the strain gage balance, and the model balancing technique, and the assistance of Mr. E. Bluestone in solving the model design problems.

B A L L I S T I C   R E S E A R C H   L A B O R A T O R I E S

REPORT NO. 994

ASPlatou/JSternberg/rf
Aberdeen Proving Ground, Md.
September 1956

THE MAGNUS CHARACTERISTICS OF A 30 MM AIRCRAFT BULLET (U)

ABSTRACT

Magnus and pitch plane data at M_∞ = 1.5 to 2.5 have been obtained on a small fineness ratio (ℓ/d = 3) body of revolution. Data have been obtained at angles of attack up to 40° under turbulent boundary layer conditions. The Magnus data are non-linear with spin and with angle of attack and the Magnus force at most spin conditions is negative in the low angle of attack region.

SUMMARY

Magnus force and pitching moment data have been obtained on a model of a 30mm aircraft bullet in the Mach number range of 1.5 to 2.5. These data cover angles of attack up to 40° and spin rates up to 45,000 RPM which include the spin rates of the prototype. The Magnus force and moment are non-linear with spin and with angle of attack and are negative in the low angle of attack range. The Magnus center of pressure is located on the rear portion of the configuration for all of the conditions where it could be accurately measured. The normal force and pitching moment are only very slightly dependent on spin.

TABLE OF SYMBOLS

Air Characteristics

a = speed of sound

U_g = Bullet muzzle velocity with respect to gun

U_a = Bullet velocity with respect to air

U_{ts} = Test section velocity

P_o = Stagnation pressure

P_{ts} = Test section static pressure

T_o = Stagnation temperature

q = Dynamic pressure = $\frac{1}{2} \rho U_{ts}^2$

ρ = Density of air

μ = Viscosity of air

Ma = Mach number

Re = Reynolds No. = $\frac{\rho u d}{\mu}$

Model and Balance Dimensions and Constants

D = Prototype body diameter

d = Model body diameter

C.G. = Center of gravity = 1.32 cal. from the base

Angles

α = Angle of attack

Γ = Gun traverse angle

ω = Bullet spin rate rad./sec (plus is clockwise looking upstream)

ν_g = $\frac{\omega d}{U_g}$ = non-dimensional spin rad/cal. (with respect to gun)

ν_a = $\frac{\omega d}{U_a}$ = non-dimensional spin rad/cal. (with respect to air)

TABLE OF SYMBOLS (Cont'd)

Forces and Moments

$$k_N = \frac{N}{\rho\, U_{ts}^2\, d^2}$$ = Normal force coefficient

$$k_m = \frac{m}{\rho\, U_{ts}^2\, d^3}$$ = Pitching moment coefficient (about C.G.)

$$k_F = \frac{F}{\rho\, U_{ts}^2\, d^2 \left(\frac{\omega d}{U_{ts}}\right)}$$ = Magnus force coefficient (plus is to left looking upstream)

$$k_T = \frac{T}{\rho\, U_{ts}^2\, d^3 \left(\frac{\omega d}{U_{ts}}\right)}$$ = Magnus moment coefficient (about C.G.) (plus is plus force ahead of the C.G.)

$$K_T = \frac{T}{\rho\, U_{ts}^2\, d^3 \left(\frac{\omega d}{U_{ts}}\right) \sin \alpha}$$ = Ballistics Magnus moment coefficient (α in radians)

$$K_T = \frac{dk_T}{d\alpha} \text{ at small } \alpha$$

INTRODUCTION

The use of spin stabilized bullets for the tail defense of very high speed bombers introduces new problems in the prediction of the bullet trajectories. In general, the bullet is to be launched from the gun at some angle to the flight path of the plane, and since the speed of the plane and the muzzle velocity of the gun are comparable, the bullet may start its flight at large angles of yaw. For a typical bullet shown in Fig. 3, initial yaw angles over 40° may be attained; further the subsequent motion may result in even higher yaw angles near the gun muzzle. To aid in predicting the bullet trajectories at these angles of attack a considerable amount of aerodynamic information for the bullet must be obtained.

It is well known that spin affects the aerodynamic forces on a body of revolution. Besides possible effects on the normal and drag forces the spin can generate an entirely new force, called the Magnus force, which acts in a direction perpendicular to the axis of the body and perpendicular to the angle of attack plane. It is also known that at small angles of attack the Magnus moment is often of great importance in determining the dynamic stability of projectiles and it seems reasonable to expect the Magnus moment to be also of importance at large angles of attack. In order to obtain knowledge of the Magnus forces at both large and small angles of attack, the instrumentation and test procedure described in this report have been developed.

We have been able to cover only a portion of the angle of attack - Mach number range shown in Fig. 1. At the lower supersonic Mach numbers the tunnel walls interfere with the flow about the model especially at the larger angles of attack, so we limited the tests to Mach numbers of 1.57, 2.0, and 2.47. Tests could have been performed at lower supersonic Mach numbers if we had a reduced model diameter. However, since the bullet is only 3 calibers long, a model diameter significantly less than the diameter chosen (2") would have forced us to place the strain gage balance downstream of the model, thereby reducing the accuracy of the

measurements. The circled points in Fig. 1 indicate the maximum angle of attack conditions at which reliable data have been obtained. Fig. 2 indicates the test Reynolds numbers compared to the free flight Reynolds numbers.

The wind tunnel model must produce the same non-dimensional spin (rad/cal. of forward travel) as the prototype in free flight. Since the prototype always leaves the gun with the same spin (ν_g), the initial non-dimensional spin (ν_a) is only dependent on the resultant velocity of the bullet, hence

$$\nu_a = \frac{\omega D}{U_a} = \nu_g \quad \frac{U_g}{U_a}$$

Fig. 1 shows the values of ν_a which are required for the 30mm bullet for which $\nu_g = .28$. The model spin rates (rad./sec) are

$$\omega = \nu_a \quad \frac{U_{ts}}{d} .$$

This corresponds to spin rates up to 45,000 RPM for the 2 inch diameter model tested at Mach No. 1.57. At Mach No. 2.47 the same model must spin at 36,000 RPM.

II EXPERIMENTAL PROCEDURE

A. The Model and Instrumentation

The two inch diameter model of the 30mm aircraft bullet is shown in Fig. 3. All external dimensions are proportionately scaled from the prototype except for the grooves in the rotating band. The model grooves are of the proper width, depth, and cant, however the "slurring over", Fig. 4, which is created on one side of the groove as the prototype moves in the gun barrel, is not duplicated. The "slurring over" would be difficult to duplicate and its effect on the Magnus data is probably small compared to the effect of the grooves themselves.

The air motor is an integral part of the model, the model forming the outside surface of the revolving portion of the motor. This portion of the motor is mounted on the bearing outer races as shown in Fig. 5. The inner races of the bearing are mounted on a cylinder which in turn is mounted on the upstream end of the model strain gage balance and supporting strut. The model is rotated by an impulse air turbine with the turbine buckets being mounted in the model base and the air nozzles, of which there are four, being mounted just upstream of the buckets on the supporting strut. An axial hole drilled in the supporting strut serves as a passage for the high pressure air to the nozzles; at the usual test conditions the flow out of the nozzles should be approximately Mach number 4. Since the nozzle air is exhausted into the tunnel, dry air from the wind tunnel storage sphere is used as the high pressure source.

For these tests sufficient power to operate the motor easily was obtained by using a supply pressure of 175 psi. Under the test conditions the motor has a starting torque of 1.2 in. lbs. and develops .5 HP at 45,000 RPM. The acceleration time from 0 to 45,000 RPM is approximately 30 sec.

A spring is used to preload the bearings so that the bearings are subjected to a thrust at all times. The preload appears to confine the ball rotation to one axis, because a track is worn into the ball surface after several thousand revolutions, Fig. 6. A thermocouple is mounted near the forward end of the strut so that the temperature rise of the strut can be measured when the model is spun. While breaking in a set of bearings, the appearance of a well worn track is indicated by a leveling off or decrease in the temperature of the forward end of the strut. After several minutes of running at low speeds the temperature stops rising and may in the case of an extremely good bearing start decreasing. Bearings are broken in by measuring the strut temperature at 10,000 and 20,000 RPM and no bearings are run at higher speeds until no temperature increase is obtained at the low speeds. If the preload is

removed from the bearing, the bearing balls will reorient themselves and a rebreaking in one of the bearings is necessary.

Measurement of the temperature of the forward end of the strut is also necessary during the tunnel tests for it indicates the condition of the bearings during any one spin period. If the temperature rise becomes excessive or if the temperature of the strut rises above 150° F the bearings are rinsed in a clear solvent and regreased. The 150 degree F limit was found to be just under the temperature at which freezing of the bearings might occur.

Two permanent magnets are mounted near the base of the model (see Fig. 5). As the model rotates, the magnetic field generates a current in a coil mounted on the stationary strut. Using suitable circuitry, the resultant coil signal is converted into a signal proportional to the RPM of the model.

Dynamic balancing of the model is accomplished using a sensitive balancing rig which determines the location and amount of metal to be removed from both the nose and tail of the model. The balancing reduces the wear on the bearings especially at resonant speeds and reduces the strain gage signal oscillations at resonant speeds. Necessarily, readings are not taken near the resonant points.

In practice, the strain gage hinge lines were not positioned exactly as desired. The angles and lengths, which are needed to sort out the pitching and yawing moments, are measured by means of a static calibration described in Appendix I. The desired moments could then be determined by solving a set of four simultaneous equations. As will be noted later, however it was possible to considerably simplify the reduction procedure.

Temperature compensation of the strain gage bridges was accomplished by varying the resistance of one of the bridge legs until the bridge indicated no unbalance when the temperature of the beam was

changed. During test, temperature non-uniformity of the beam caused by heat from the bearings might still cause trouble, so as a check, the bridge unbalance was observed as the model spin varied from 45,000 RPM to 0 under no flow conditions. No bridge unbalance was found, except at resonant speeds, so the method of temperature compensation was considered satisfactory.

The model was tested on two different support systems. The power lead lengths for each of these installations differed, and it was necessary to correct the bridge sensitivity for the differences in the power lead resistances.

B. Model Support and Tunnel Interference

Comparisons of wind tunnel base pressures with free flight base pressures on the same model at the same test conditions have shown that if the wind tunnel support system is made small enough, the tunnel and free flight measurements are in reasonable agreement. However, in most cases, the model loads are too large to allow the use of a support system which does not change the wake flow. On a cylindrical body at small angles of attack, with a convergent wake, the change in the upstream flow is of negligible importance. If the support system interference is large enough to diverge the wake flow the resultant shock wave at the model base may cause separation of the boundary layer on the model surface. It would then be possible for the support system to affect the flow over an extensive region of the body. If this separation does not occur, then measurements of the model forces, with the exception of the base force should be valid.

As long as the flow relative to the model surface is supersonic, the Magnus force and moment measurements should be free of support interference. When the flow is supersonic relative to the model, shock waves arising from the irregularities of the model surface near the base, are clearly visible in the Schlieren photographs. Fig. 7 shows the model at an angle of attack where the flow is everywhere supersonic. In Fig. 8

the flow separates on the top side of the model near the nose and there is a very extensive subsonic wake. As will be described below the photographic observations were supplemented with normal force and pitching moment measurements on a non-rotating model. As could be expected, the development of an extensive wake caused large changes in the model forces.

A limited series of measurements were made at $M_\infty = 2.0$, $\alpha = 10^\circ$, and 20° to confirm the supposition that the Magnus forces would be independent of the wake flow. The wake flow was altered by placing rings on the strut just aft of the model base and no changes in the Magnus force were found.

The tests of the various support configurations were made by measuring the normal force and pitching moment on a non-spinning model. Magnus force measurements on a spinning model with a series of different struts would have been very time-consuming and expensive; however, it was possible that the non-spinning tests might not be satisfactory. The model spin alters the boundary layer on the model in a complicated way, and it is possible that the altered boundary layer might be more susceptible to separation than the boundary layer on the non-spinning model. However, in the latter case, the normal force or pitching moment should have been significantly affected by the model spin; all of the test data indicated a negligible influence of spin on the pitch plane forces.

At large yaw angles, the direction of the wake axis is intermediate between the strut axis and the free stream flow direction. We thought that the strut interference might be minimized if the strut axis coincided with the wake axis, because then the initial portion of the strut would be in a low speed flow and the pressure changes produced by the strut would be relatively small. Fig. 9 shows the strut arrangement that was used to vary the angle between the strut axis and the model axis. Fig. 10 shows how these different struts were connected to the tunnel angle of attack system to allow testing of the model in a given angle of attack range with a series of different struts. The Schlieren pictures suggest that the development of a subsonic region on the model

was largely determined by flow interference from portions of the model support system other than the strut at the model base. In particular, interference from the downstream portion of the strut and the piece connecting the strut to the angle of attack system probably had as much or more to do with the resultant flow as the angle between the strut and model axis. The four Schlieren photographs (Fig. 11) at $\alpha = 40^{\circ}$, $M = 1.57$, as well as the peculiar rise in the pitching moment curve near that angle of attack, (see Fig. 13) indicate the development of large wakes although the degree of separation differed for the different struts. With the $B = 0^{\circ}$ strut, there was a reflected shock from the Mach intersection near the wall, which intersected the wake a little over one model diameter from the base. With the $B = 30^{\circ}$ strut, the reflected shock struck the wake much further downstream and the degree of separation appeared to be much reduced. Fig. 12 shows the same four strut configurations at $\alpha = 30^{\circ}$ at $M = 1.57$. At this angle of attack both the Schlieren photographs and the pitch plane data indicated interference free results. As at $\alpha = 40^{\circ}$, the reflected shock system for $B = 0^{\circ}$ strut intersected the wake closer to the model base than the reflected shock for the other struts; however the reflected shock was still 2 1/2 model diameters from the base.

At $M = 1.57$ and $M = 2.0$, we felt there was little to choose between the several strut configurations. The presumptive evidence indicates that there was some interference present for all of the configurations above $\alpha = 32^{\circ}$ at $M = 1.57$, and $\alpha = 44^{\circ}$ at $M = 2.0$. At $M = 2.47$, the maximum α required was only 20° so that strut interference was not a problem. In view of these results, a coaxial strut was used for all of the measurements.

While the main objective of these tests was to obtain Magnus data at large yaw, we had a strong interest in obtaining accurate data at small yaw. Unfortunately, the precision we desired at small yaw could not be achieved using the tunnel angle of attack system. The support system deflects easily in the horizontal plane and further, the

attachment of the strut support to the guiding crescent is imperfect, and a small amount of inelastic movement is possible. Careful measurements showed that the uncertainty in yaw angle due to the existing side-play was not particularly important. However, when tested the model oscillated a small amount in the horizontal plane with an irregularly varying amplitude. The resultant oscillation of the yawing moments greatly reduced the accuracy of the measurements. To provide a more rigid support for the model, a door mount (see Fig. 16) was used at all of the Mach numbers. (See Figs. 13-15). It was still necessary, however, to make some experiments at small yaw with the tunnel angle of attack system. The door mount does not have a window for Schlieren observation and flow observations were needed to clarify some of the initial results.

Normal force and pitching moment measurements obtained using the door mount are also shown in Figs. 13-15. Flow interference appears to occur at $\alpha = 25^{\circ}$ at $M = 1.57$ and at $\alpha = 34^{\circ}$ at $M = 2.00$. The angle of attack on the door mount was changed by externally rotating a disk; the swept back double wedge support holding the model strut was connected to the disk. As the model angle of attack was increased, the angle of attack of the support also increased. Further, it simultaneously moved close to the floor of the tunnel. We believe that the resultant strong shock system caused flow separation on the model. A special model strut has now been fabricated which is bent 22° at the model base. With this new strut the support system flow disturbances should be greatly reduced and it should be possible to use the door mount over the entire angle of attack range, if desired. Actually at large yaw, since the measured forces are larger, the scatter introduced by the oscillations of the model mounted on the tunnel angle of attack system are not important.

C. Reduction of Test Data

Because of imperfections in the tunnel flow and imperfect alignment and/or tracking of the angle of attack systems that were used, the resultant angle of attack of the model with respect to the airstream is, in general, not in a vertical plane through the tunnel axis. Therefore, the

yawing moment at no spin will not be zero and will vary with the model angle of attack. In addition, there will be an apparent yawing moment because the yawing moment hinge lines are not parallel and in the plane of the angle of attack. During installation of the model in the tunnel an adjustment of the balance roll angle is made to limit, as far as is practicable, these no spin yawing moments.

The deflection of the model support system under load introduced some possible additional complications in obtaining the Magnus forces. For instance, if the pitch plane forces changed substantially with spin, the angle of attack might vary significantly with spin. Fortunately, as was noted previously, the pitch plane forces were practically invariant with spin (Fig. 17-19). Similarly, the Magnus forces themselves will deflect the support system in the horizontal plane thereby changing the direction of the resultant angle of attack. Hence there will be yawing moments due to the inclination of the normal force vector which have to be subtracted from the total yawing moments to obtain the Magnus moments themselves.

Strut deflection constants were obtained for vertical and horizontal loads. The pitch plane constants were used to correct the vertical component of the angle of attack and the lateral constants were used to determine the yawing moment due to the inclination of the normal force vector. The Magnus force in these tests was always small so that the change in the lateral component of the angle of attack caused by the Magnus force was always small (.01 degrees was the maximum deflection computed). Hence the apparent Magnus force due to the inclination of the normal force vector can be shown to be

$$\Delta N = N \frac{\sin \Delta\beta}{\tan \alpha}$$

where $\Delta\beta$ is the change in the lateral component of α.

The resulting error in the Magnus force is within the experimental accuracy and therefore was not included in the reduction.

The normal force contribution to the measured yawing moment was computed in several critical cases and was found to be negligible. As a result, it was possible to determine the Magnus data by simply subtracting the yawing moment at zero spin for each angle of attack.

III. RESULTS

The first experiments were made at M = 2.0 at small angles of attack an very curious results were obtained. The Magnus moments could be repeated consistently at various spin rates, but the zero spin yawing moment was different almost every time the model stopped. The spread in the zero spin yawing moment values was too large to disregard when compared with yawing moment variations observed with changes in spin rate. Also the Magnus force varied non-linearly with spin and extrapolation of the data to zero spin appeared hazardous. It was soon found that the yawing moment was a single valued function of the roll angle at which the model happened to stop during each test. Shadowgraphs of the model (see Fig. 20) at different roll angles suggested that the boundary layer transition on the model surface was largely controlled by small imperfections of the model surface, since the position of transition on the top and bottom elements, as shown in the photographs, was different for different roll angles. Even if the model were perfectly made and at zero angle of attack, it would be unlikely that the transition would occur at the same axial position all around the model because of the influence of non-uniformities in the tunnel flow. But in the latter case, the transition pattern would have remained fixed with respect to the tunnel coordinates and so would not have been troublesome. A difference in the axial position of the boundary layer transition around the model implied a difference in boundary layer displacement thickness at downstream axial stations. The "effective" body would then not be at zero lift, and there would be some pitcHing and yawing moment on the model. Such yawing moments on this model are probably larger than those that would be found on a smoothly contoured model because of the presence of the rotating band. Fig. 20 shows that when the boundary layer is laminar ahead of the rotating band that boundary layer separation occurs well upstream of the rotating band.

It is not possible to calculate with any reliability from the photographs what changes in moment should have been produced, since the data are necessarily incomplete. Estimates indicate that small changes in the effective angle of attack of the order of $.02^\circ$ - $.03^\circ$ would have been sufficient to account for the measurements. At any reasonable spin rate, any force dependence on roll angle would be averaged by the instrumentation. As the angle of attack is increased, the effect of the angle of attack on transition on the body becomes more and more important. Above about 7°, the dependence of the transition on the model roll angle becomes negligible. When the Reynolds number was increased from .62 to $.94 \times 10^6$, the transition occurred fairly well forward on the body (Fig. 21). The resultant yawing moment variation, which was about half the variation experienced at the lower Reynolds number was about the same magnitude as the uncertainty in reading the data, and was considered to be acceptable. Similar results were achieved at the lower Reynolds number by using a boundary layer trip ring near the base of the ogive.

The data obtained at the higher Reynolds numbers at three Mach numbers, 1.57, 2.00, and 2.47, are shown in Figs. 22-24. The maximum value of the spin parameter $\frac{\omega d}{U}$ was approximately the same as the $\frac{\omega d}{U}$ values for the shell when it has the air Mach numbers shown, at launching. It is seen that the Magnus force reverses direction at small angles of attack. These low angle of attack tests were rerun several times to confirm that the reversal was definitely present. Furthermore, it is clear that at small angles of attack the Magnus forces and moment vary non-linearly with spin. Although the data above $10\text{-}15^\circ$ are not shown, in Figs. 22-24, the Magnus force and moment are reasonably linear with spin and can be obtained from Figs. 25-27.

Figures 25-27 are cross plots of the data at the free flight values of the non-dimensional spin parameter. As would be expected from Figs. 22-24, the Magnus force is also non-linear with yaw. The data at all three Mach numbers indicate that the center of the pressure of the Magnus forces changes

with angle of attack and that the Magnus force coefficient reaches a peak value at about 15 - 20° α. At angles of attack below 5°, the accuracy of the center of pressure determination is poor and so it has not been entered on the graphs. The data at M = 1.57 and 2.00 also indicate that the Magnus force coefficient approaches a constant value at about 30° α. Certainly it is not safe to extrapolate these data to still larger angles of attack.

IV. COMPARISON WITH THEORY

As far as we know, no adequate theory exists at the present time for predicting the Magnus forces on the model used in these tests. The principal theoretical work that has been done has been directed towards calculating the Magnus forces at small angles of attack, with laminar boundary layers, on very simple body shapes. It is found that the boundary layer on the model is altered by the combined effects of angle of attack and spin. The resulting displacement thickness distribution is not symmetrical with respect to the vertical plane, so that Magnus forces can be produced. Also there may be a significant force contribution arising from asymmetry of the skin friction forces. The existing solutions [1,2] assume an incompressible flow and do not account for the actual boundary layer development on the nose. In addition, because of the disturbance produced by the rotating band, at Mach numbers of 1.57 to 2.47, we were not able to test with a laminar boundary layer over the whole model length at any angles of attack.

Figures 22-27 show that at angles of attack less than 5°, the Magnus force is negative, opposite in sign to the small angle force predicted for the laminar boundary layer case. The large B.R.L. free flight range has also obtained indications of negative Magnus forces (see free flight comparison section) on this configuration. However, measurements at the Naval Ordnance Laboratory on bodies with greater length to diameter ratios (about 7) do not show negative Magnus forces. This may be caused by different boundary layer conditions or by the larger fineness ratio. As yet we have been unable to determine the cause of this behavior.

The source of the Magnus forces at large angles of attack is probably entirely different. The normal forces on non-rotating bodies are reasonably well described using the ideas of H. J. Allen[5] with further refinements by Kelly[4]. If we apply these ideas to the prediction of the Magnus force at large angles of attack, we have to relate the Magnus force on a given section of the body to the Magnus force on a spinning cylinder oriented normal to the flow. The "normal" velocity for each section is taken to be the component of the free stream velocity normal to the body axis. Further, the Magnus forces on the sections have to be related, not to the steady state Magnus forces on a cylinder, but rather to the force on a rotating cylinder, impulsively started from rest, before it has developed the steady state force. The forces on forward body sections correspond to short travel distances for the cylinder, the rearward body sections to relatively large travel distances for the cylinder. At any angle of attack, the steady state forces may finally be reached on the body if the body is long enough. Unfortunately, the required low speed starting data are not available.

Further, the whole picture should change at large free stream Mach numbers and angles of attack because the Mach number component normal to the axis will approach and may exceed unity. The development of Magnus forces on a cylinder normal to the flow should be markedly dependent on the flow Mach number. At low speeds, the cylinder rotation causes the point of boundary layer separation to differ on the top and bottom of the cylinder. As a result, the vorticity of opposite sign shed at the top and bottom is not equal and there is a net amount of vorticity of one sign shed in the cylinder wake. As this happens, a circulation of the opposite sign develops around the cylinder and the pressure distribution over the whole cylinder is altered resulting in a Magnus force. When the flow is supersonic, unequal vortex shedding in the wake has a much more restricted field of influence, since its effect is restricted to the subsonic portion of the flow field, except in so

far as it may alter the points of separation of the boundary layers. The Magnus force that results is then due to a change of pressure over a small portion of the cylinder. Furthermore, at low speeds, a relatively large amount of time is required to establish the steady state force since time must be allowed for the development of the starting vortex and then its subsequent movement downstream. At supersonic speeds, the rate of approach to steady state values will depend on the relative importance of the spin and the wake conditions in determining the separation points on the cylinder. If the spin is dominant, then a steady state pressure distribution on the cylinder would be reached very rapidly.

Futher, most of the experiments that have been performed on rotating cylinders have either been at very low Reynolds numbers or in the transition region. Data for a turbulent boundary layer would be more appropriate for the type of model used in these tests.

V. FREE FLIGHT COMPARISON

This same 30mm shell has been fired in the BRL Free Flight Aerodynamics Range. The normal range reduction technique, which is based on the assumption that the forces and moments are linear with spin and angle of attack, would be clearly unsatisfactory in this case. Recently C. H. Murphy[6] has developed a method for deducing the aerodynamic coefficients from a free flight firing when the coefficients are non-linear with angle of attack. In its simpler form, the method requires a cubic or quintic fit to the actual Magnus moment curve. In spite of the fact that the experimental curve cannot be readily approximated in this way, Murphy has analysed the range results and has obtained a Magnus moment curve which is qualitatively similar to the wind tunnel curve. The Magnus moment reverses sign at about the same angle of attack and also reaches a maximum at a moderately large angle of attack.

VI. CONCLUSIONS

The following conclusions can be drawn from these data:

1. The normal force and pitching moment are only slightly dependent on spin.

2. The Magnus force is non-linear with angle of attack, and at all except the very high spin rates the force and moment change sign at the low angles of attack.

3. The Magnus force and moment do not become linear with spin until an angle of attack between 7 1/2° and 15° is reached. The angle of attack for linearity decreases as the Mach number increases.

4. The Magnus force center of pressure is located behind the center of gravity.

5. The Magnus force and moment decrease as the Mach number increases.

6. The Magnus force and moment are negative at small angles of attack and moderate spin rates. For these data, boundary layer transition occurred before the base of the ogive.

7. A maximum in Magnus force and moment was reached between 15-20° α and the Magnus forces varied little with α near $\alpha = 30°$. In this larger angle of attack range, the results appeared to be independent of Reynolds number changes produced by changing the tunnel pressure level by a factor of 2.

A.S. Platou　　J. Sternberg

A. S. PLATOU　　J. STERNBERG

VII. REFERENCES

1. Martin, J. C. - "On Magnus Effects Caused by Boundary Layer Displacement Thickness on Bodies of Revolution at Small Angles of Attack". BRL Report 870.

2. Kelly, H. R. - "An Analytical Method for the Magnus Forces and Moments on Spinning Projectiles". NOTS T.M. 1634

3. Allen, H. J., Perkins, E.W.-"A Study of the Effects of Viscosity on Flow over Slender Bodies of Revolution". NACA Rep. 1048.

4. Kelly, H. R. - "The Estimation of Normal Force and Pitching Moment Coefficients for Blunt-Based Bodies of Revolution at Large Angles of Attack". NOTS T.M. 998

5. Luchuk, W., Sparks, W. - "Wind Tunnel Magnus Characteristics of the 7 Cal. A.N. Spinner Rocket". NAVORD Rept. 3813

6. Murphy, C. H. - "The Measurement of Non-Linear Forces and Moments by Means of Free Flight Tests". BRL Rept. 974.

VIII. FIGURES

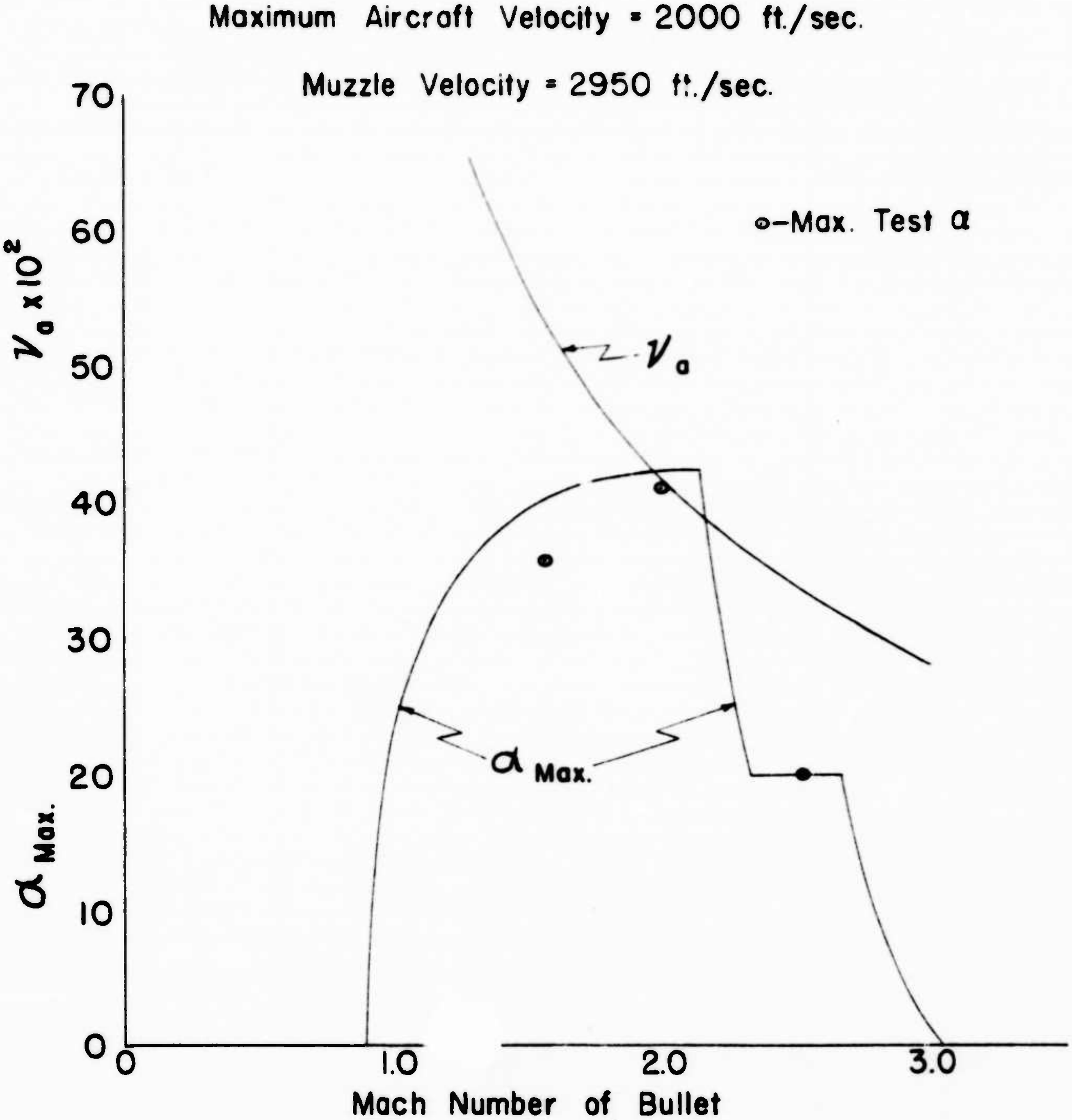

FLIGHT CONDITIONS FOR 30 MM AIRCRAFT BULLET

FIG. 1

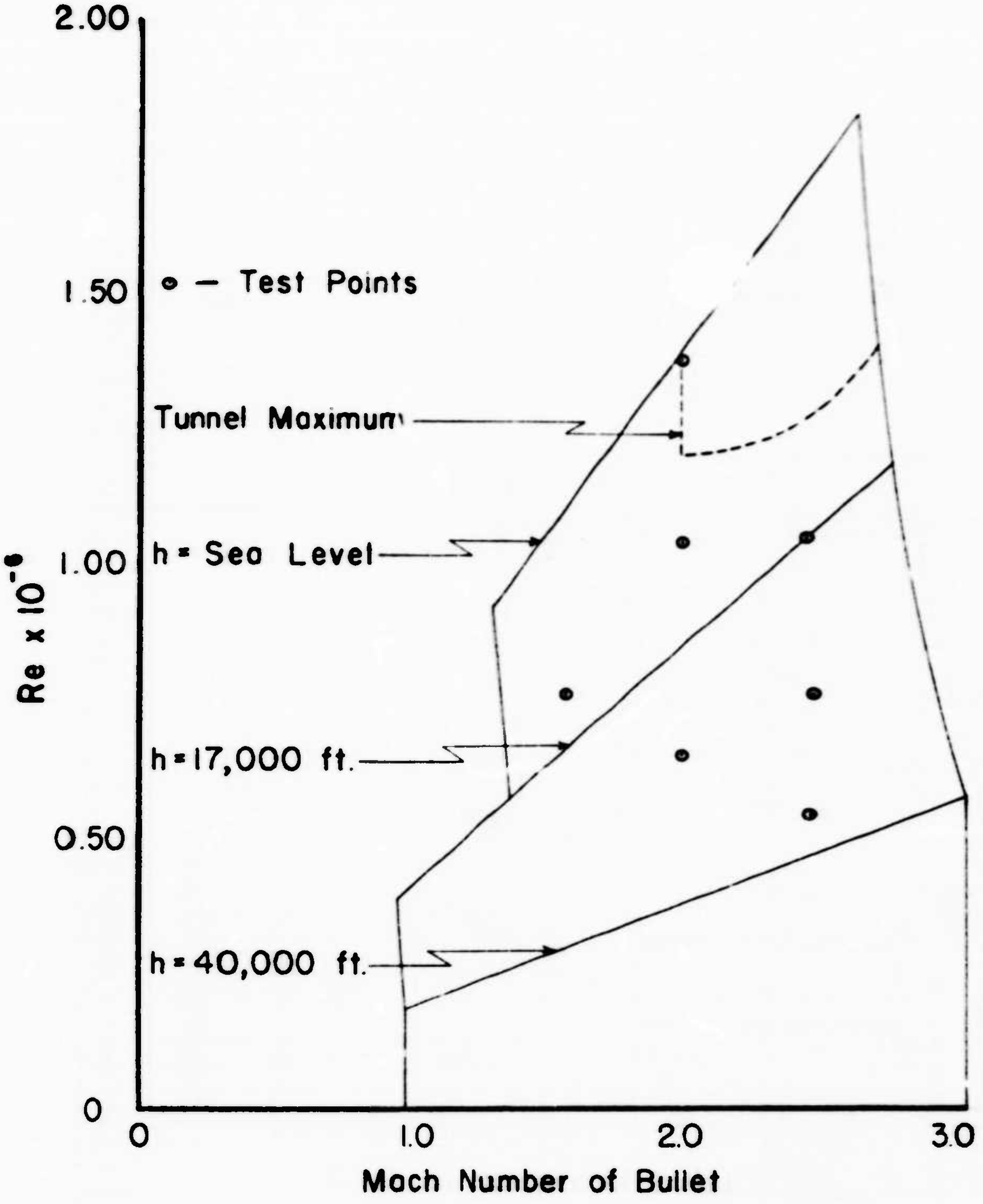

FLIGHT REYNOLDS' NUMBER FOR 30 MM AIRCRAFT BULLET

FIG. 2

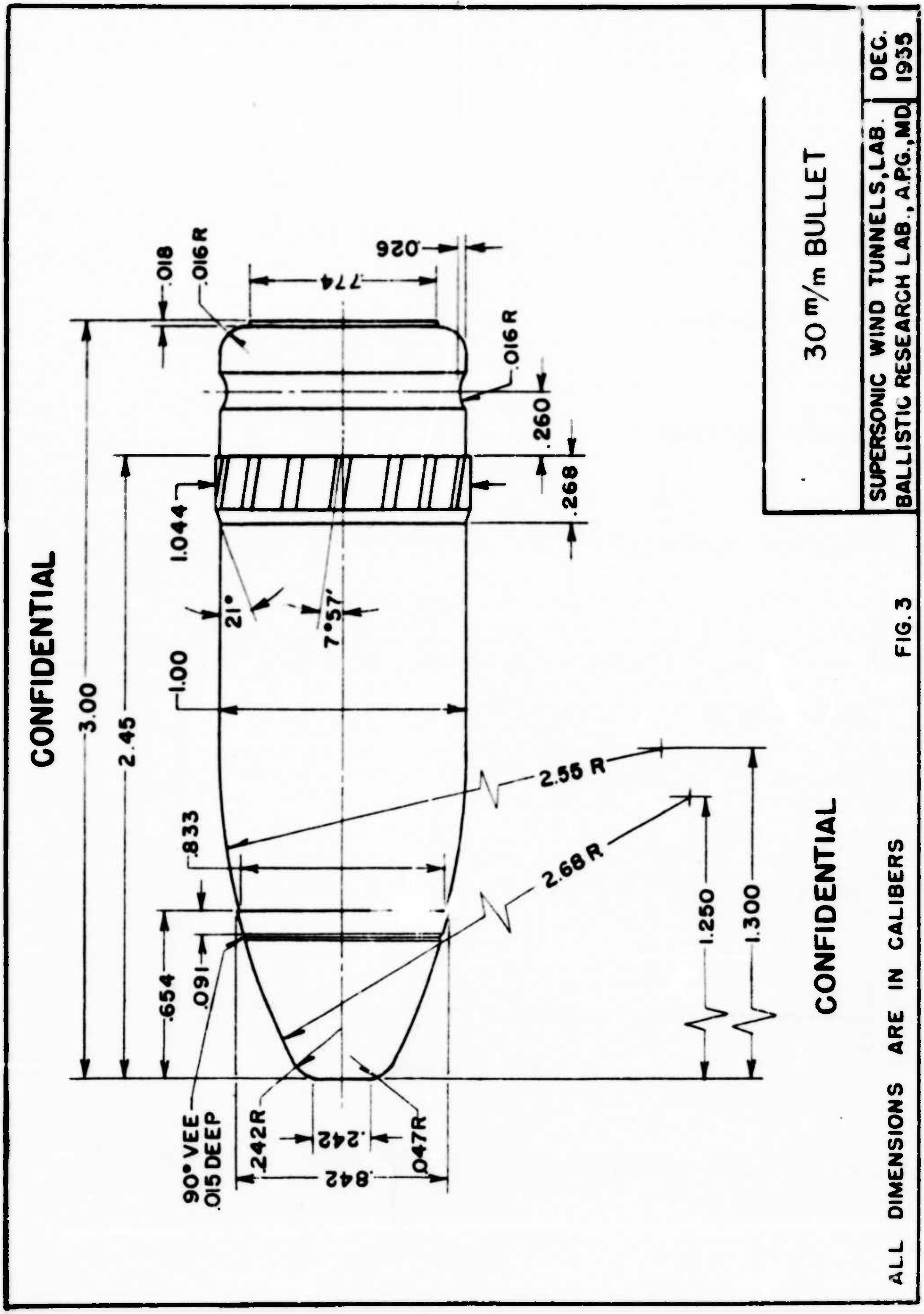
CONFIDENTIAL
30 m/m BULLET
SUPERSONIC WIND TUNNELS, LAB.
BALLISTIC RESEARCH LAB., A.P.G., MD.
DEC. 1955
.018
.016 R
.774
.026
.016 R
.260
.268
1.044
21°
7°57'
1.00
3.00
2.45
2.55 R
2.68 R
.833
.654
.091
1.250
1.300
90° VEE
.015 DEEP
.242 R
.242
.047 R
.842
CONFIDENTIAL
ALL DIMENSIONS ARE IN CALIBERS

FIG. 3

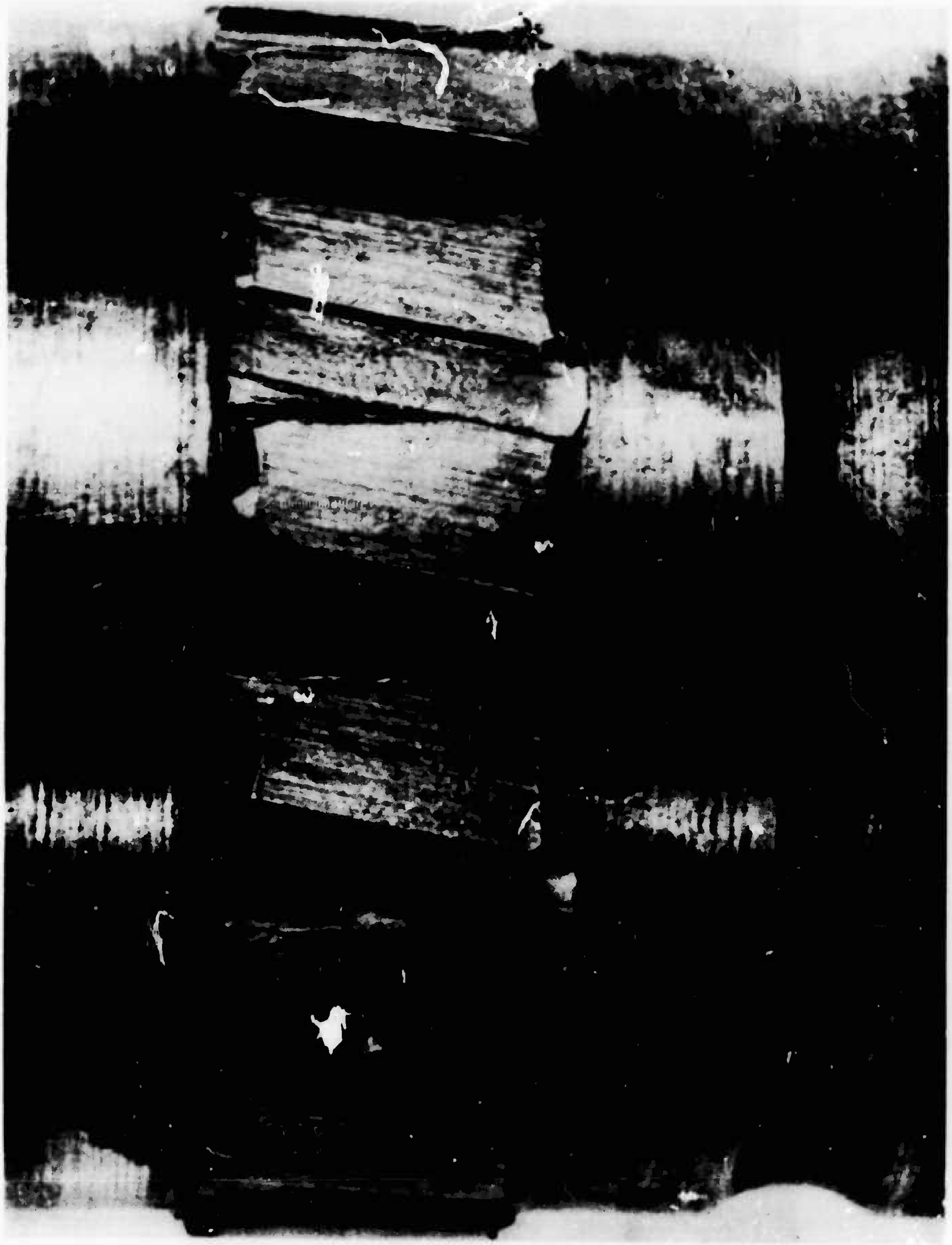

Figure 4. Photograph of 30mm Aircraft Bullet Rotating Band Grooves.

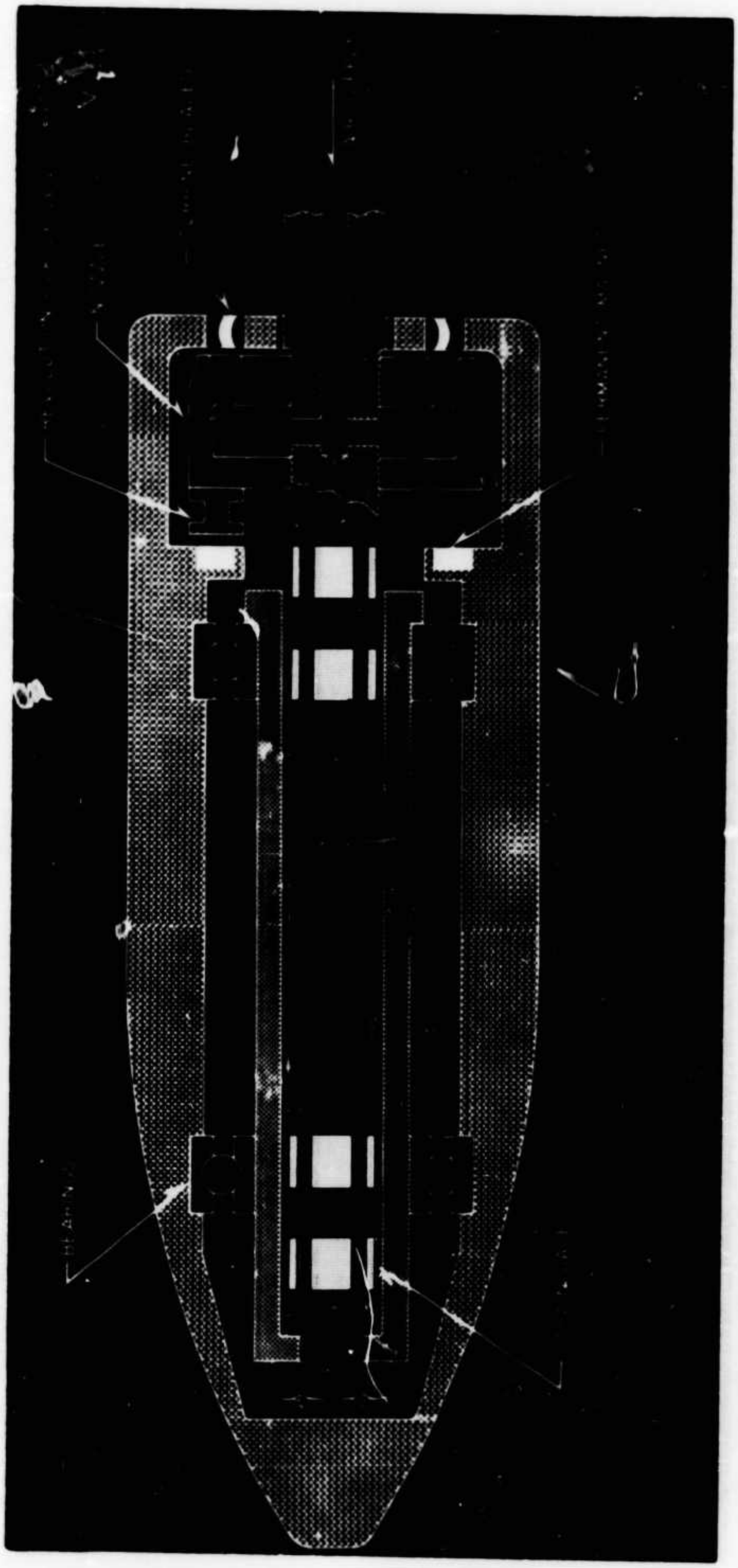

Figure 5. Spinning Model - Instrumentation.

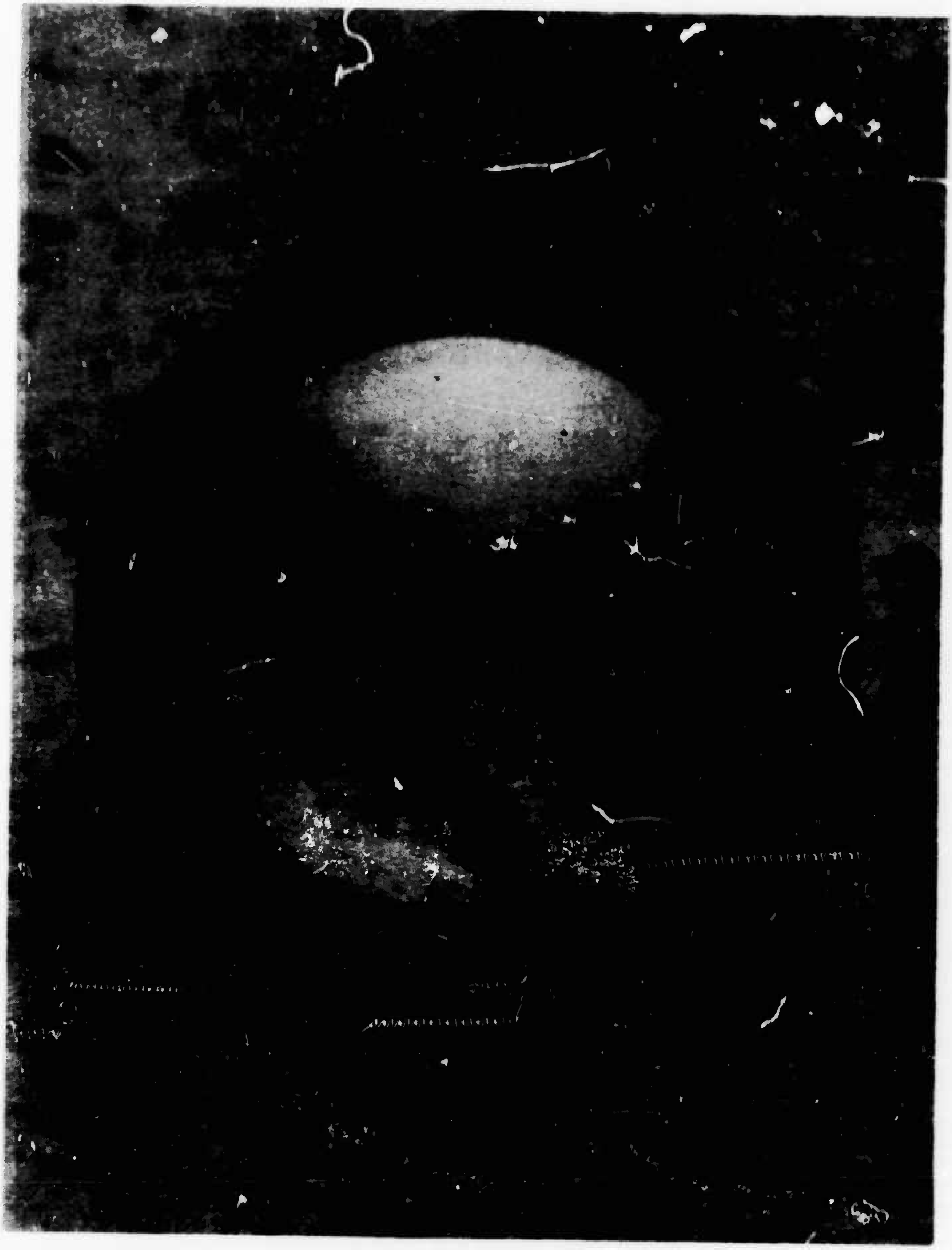

Figure 6. Ball Bearing after Break-in Period.

Figure 7.

Figure 8.

CONFIDENTIAL

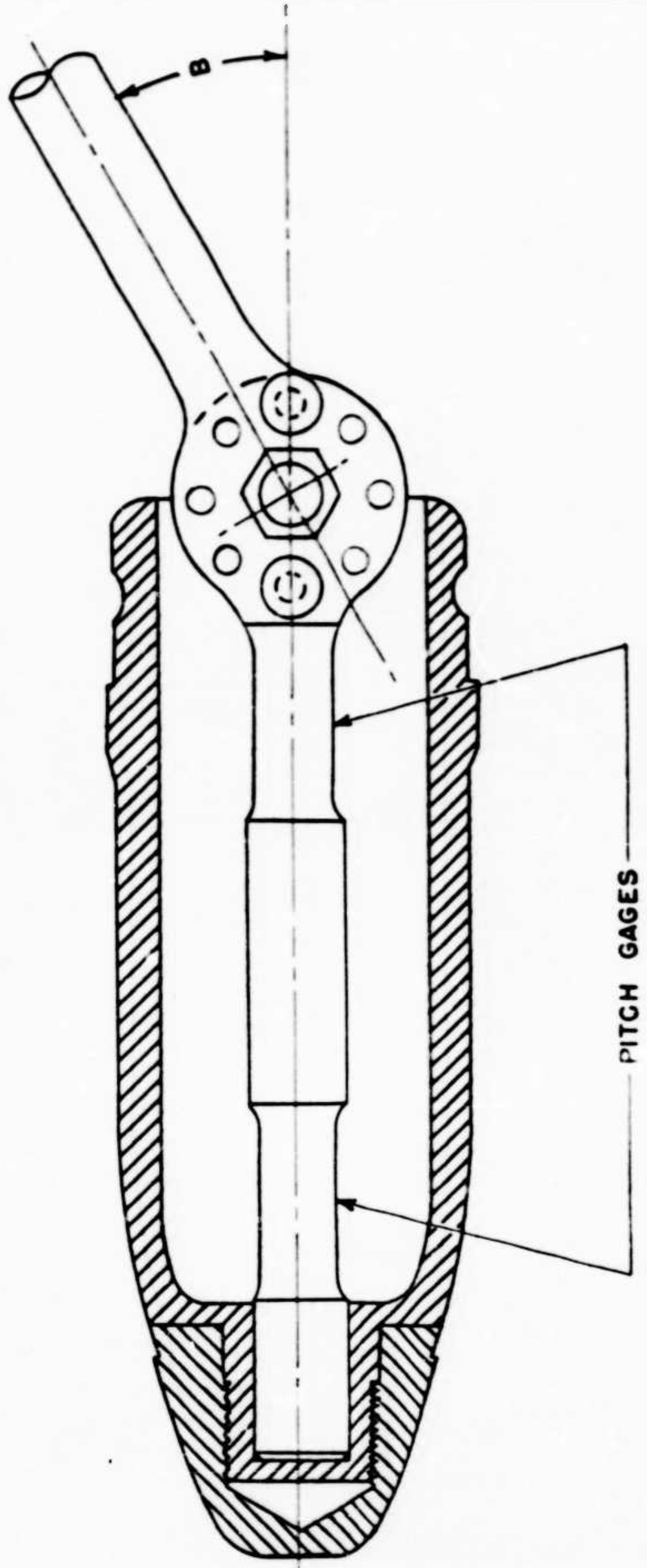

SUPPORT INTERFERENCE SERIES

SUPERSONIC WIND TUNNELS, LAB.
BALLISTIC RESEARCH LAB., A.P.G., MD

DEC. 1955

FIG. 9

NOTE:

B CAN BE SET TO 0,° 10,° 20,° 30°

CONFIDENTIAL

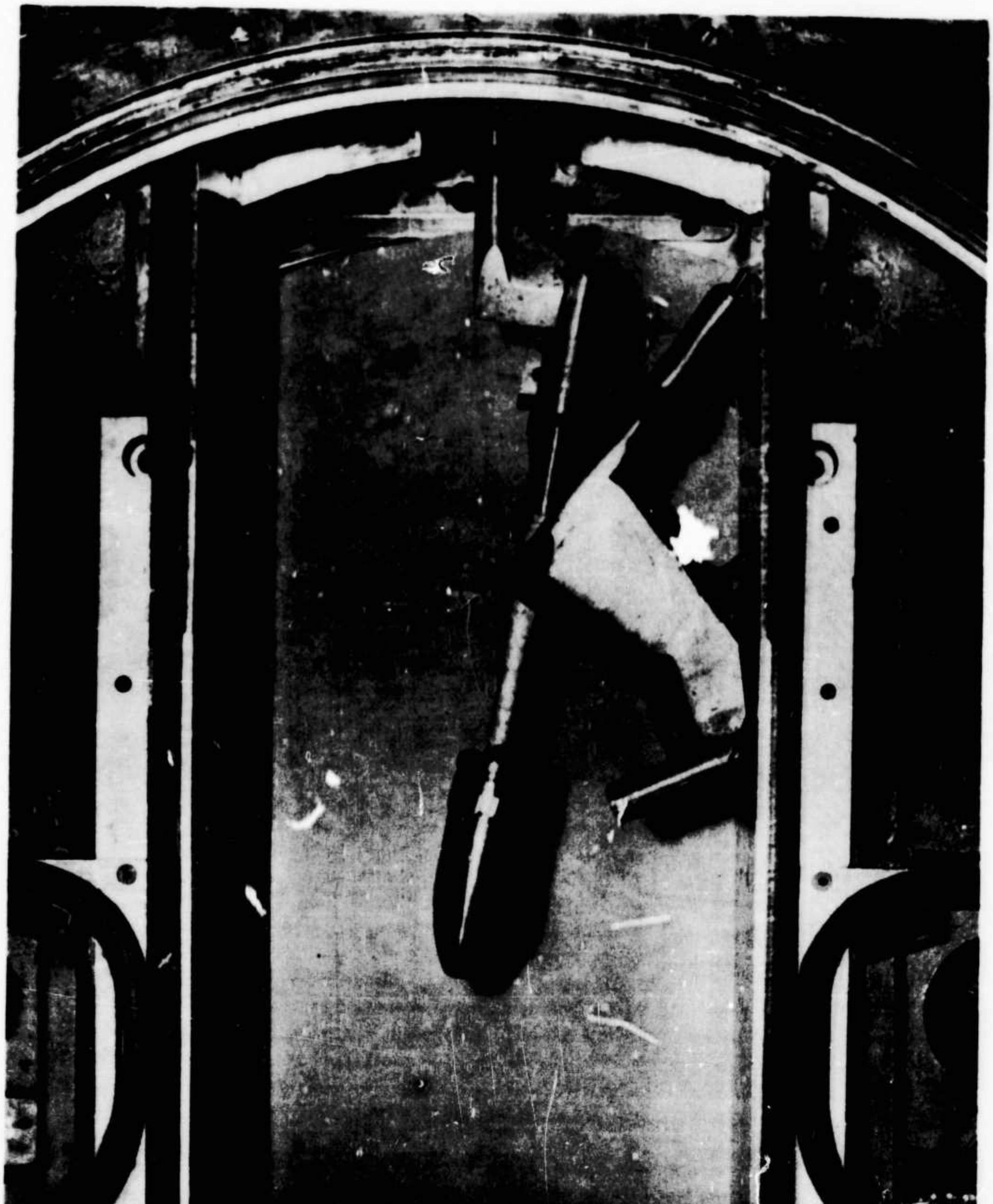

Figure 10. 30mm Aircraft Bullet Model Mount on the Tunnel Angle of Attack System showing the 10° and 32° Offset Strut Supports.

Figure 11. Schlieren Picture of the 30mm Bullet Using a 0° Swept Strut, Ma = 1.57 α = 40°.

Figure 11. Schlieren Picture of the 30mm Bullet Using a 10° Swept Strut, Ma = 1.57 α = 40°.

Figure 11. Schlieren Picture of the 30mm Bullet Using a 20° Swept Strut, Ma = 1.57 α = 40°.

Figure 11. Schlieren Picture of the 30mm Bullet Using a 30° Swept Strut, Ma = 1.57 α = 40°.

Figure 12. Schlieren Picture of the 30mm Bullet Using a 20° Swept Strut, Ma = 1.57 α = 30°.

Figure 12. Schlieren Picture of the 30mm Bullet Using a 30° Swept Strut, Ma = 1.57 α = 30°.

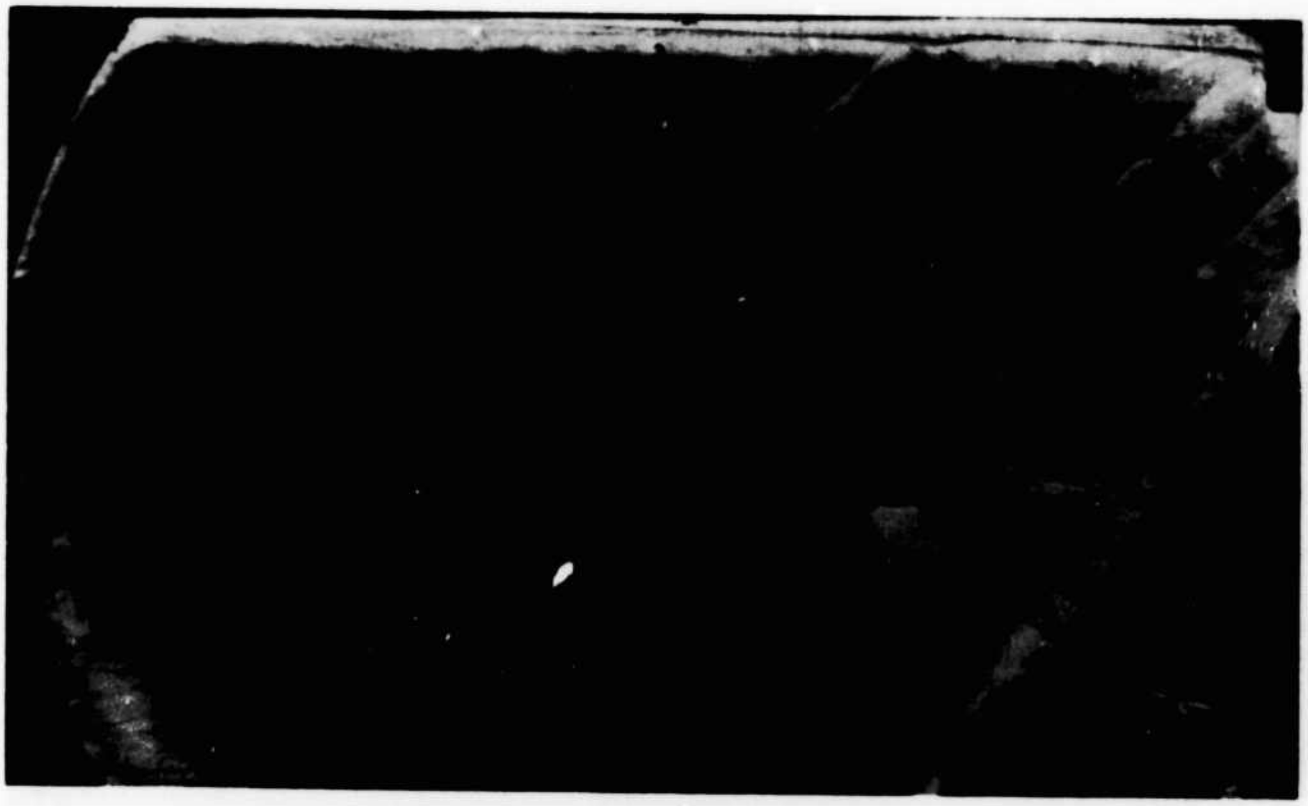

Figure 12. Schlieren Picture of the 30mm Bullet Using a 0° Swept Strut, Ma = 1.57 α = 30°.

Figure 12. Schlieren Picture of the 30mm Bullet Using a 10° Swept Strut, Ma = 1.57 α = 30°.

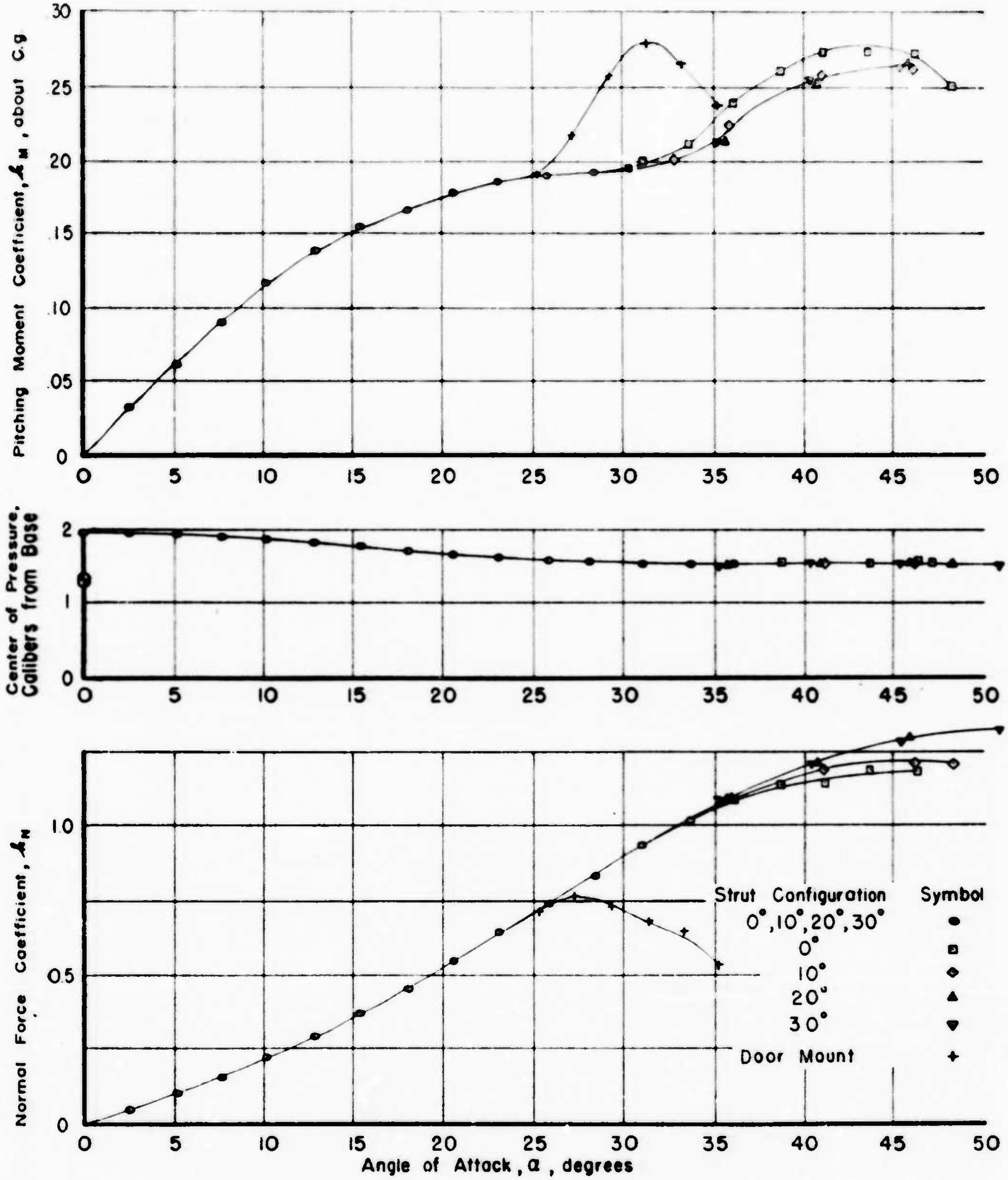

SUPPORT AND TUNNEL INTERFERENCE

Mo = 1.57

Re = 84 x10⁶

FIG.13

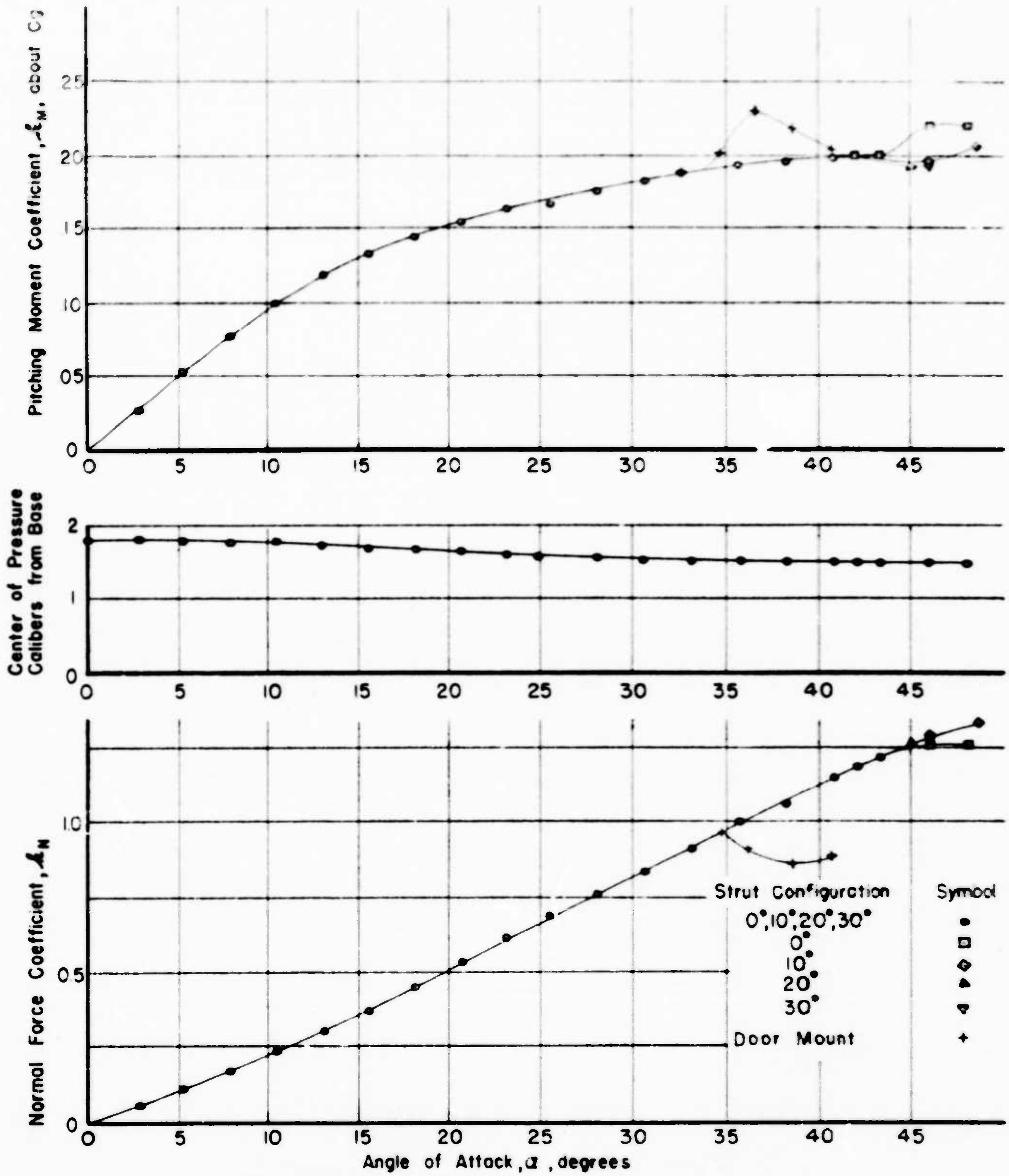

SUPPORT AND TUNNEL INTERFERENCE

Mo = 2.00

Re = .71 x 10^6

FIG. 14

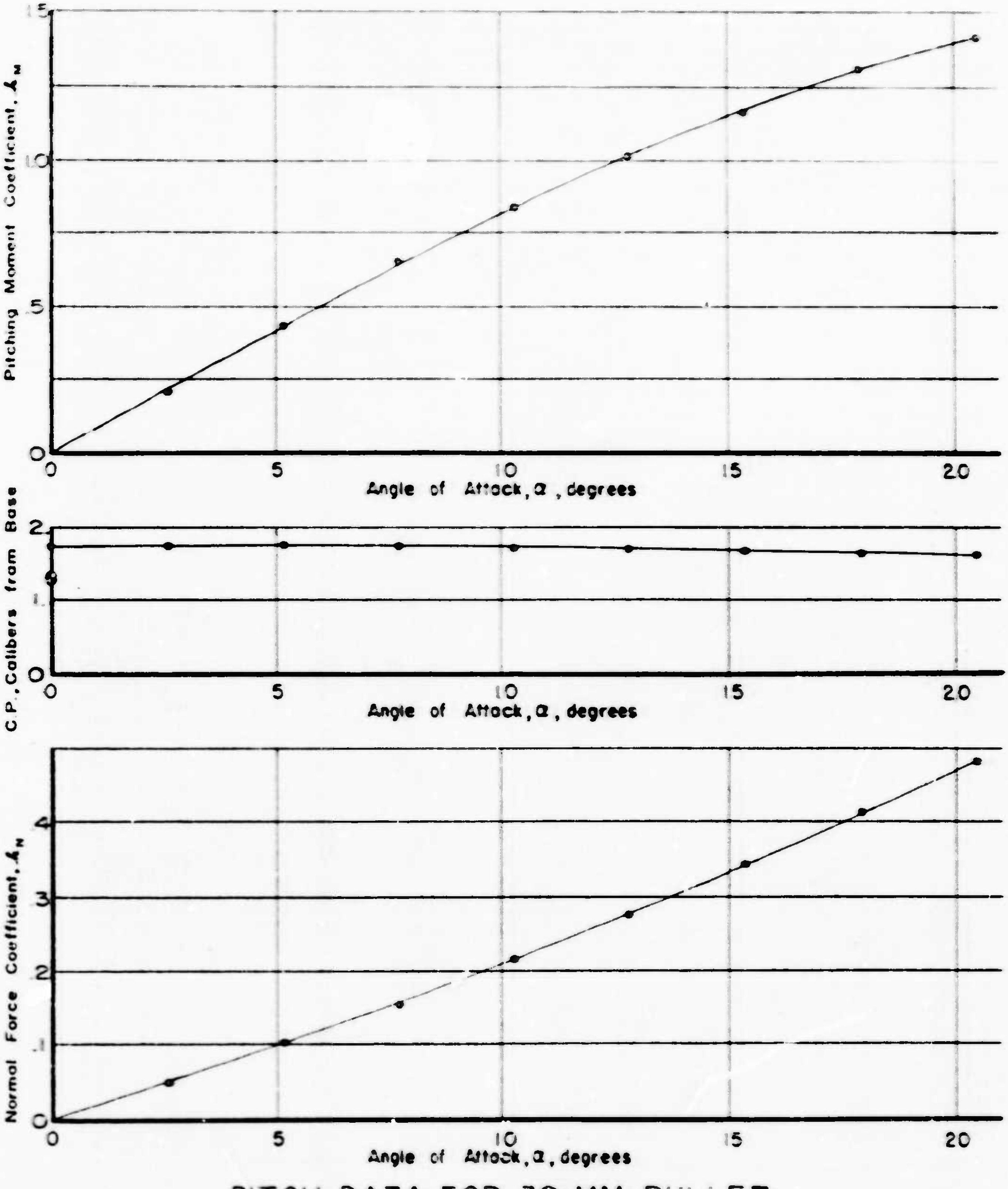

PITCH DATA FOR 30 MM BULLET

Ma = 2.47

Re = 76 x 10⁶

FIG. 15

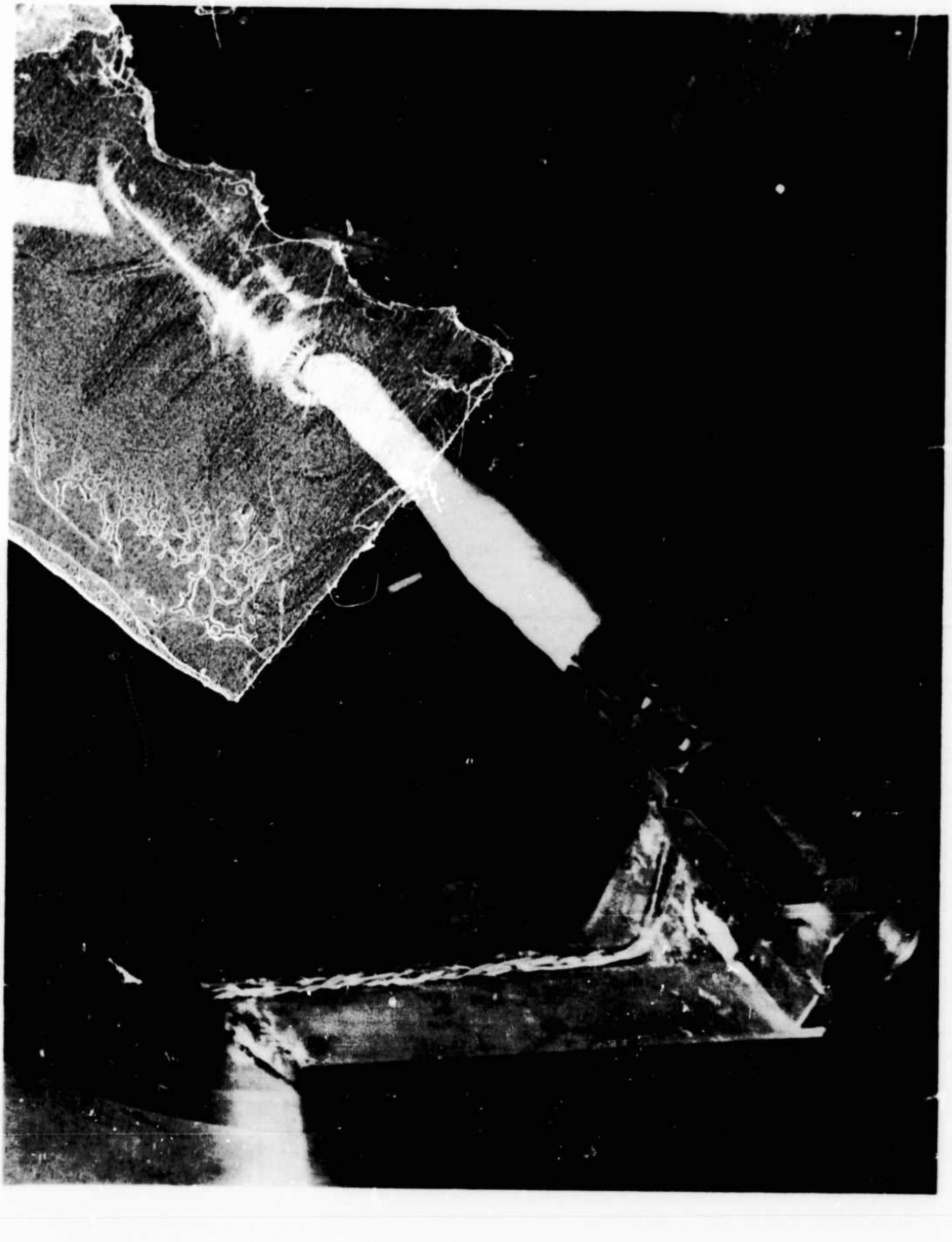

Figure 16. 2" Dia. Spinning Model Mounted on the Original Door Mount.

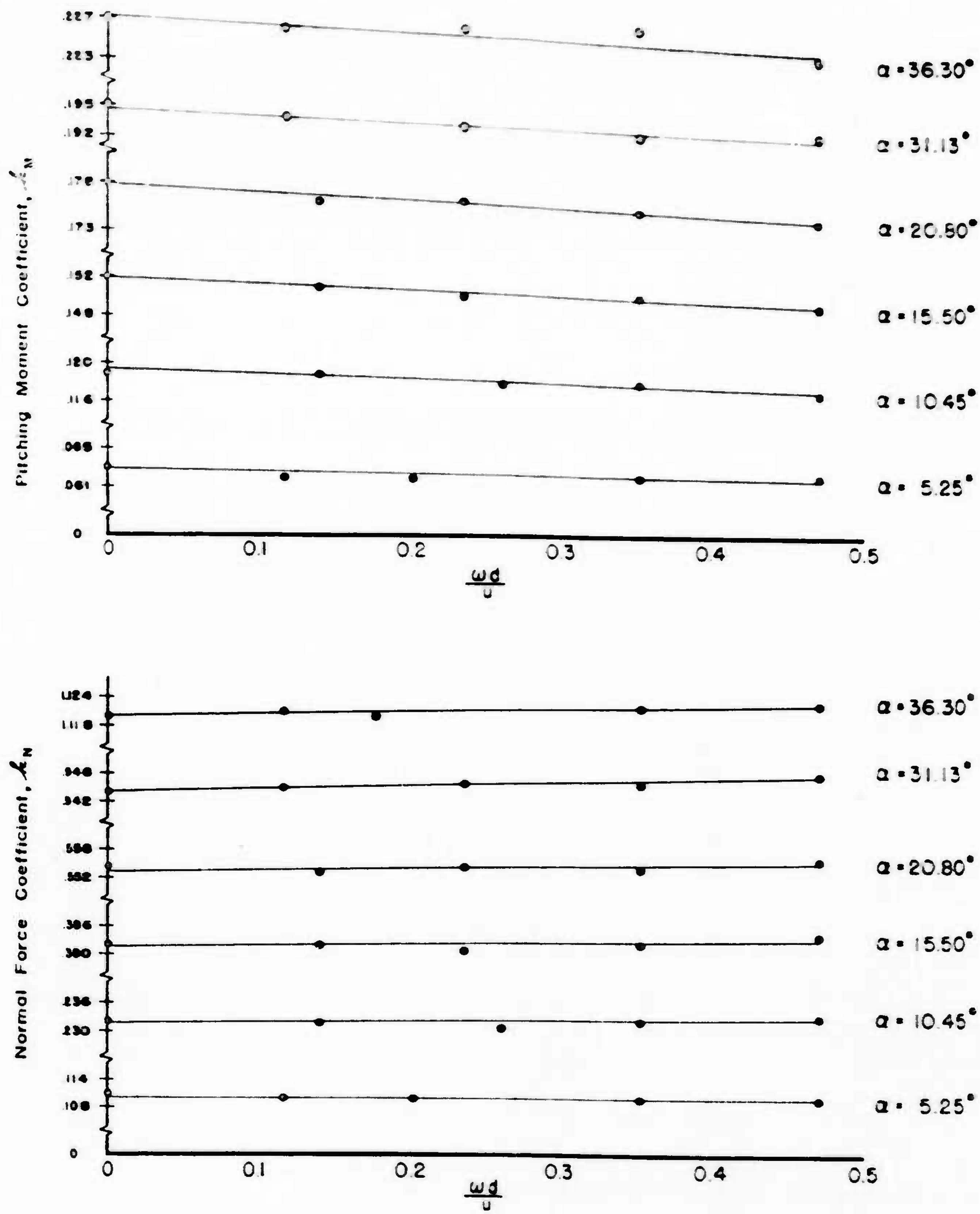

PITCH DATA VARIATION WITH SPIN FOR 30 MM BULLET

Mo = 1.57

Re = .75 x 10^6 FIG. 17

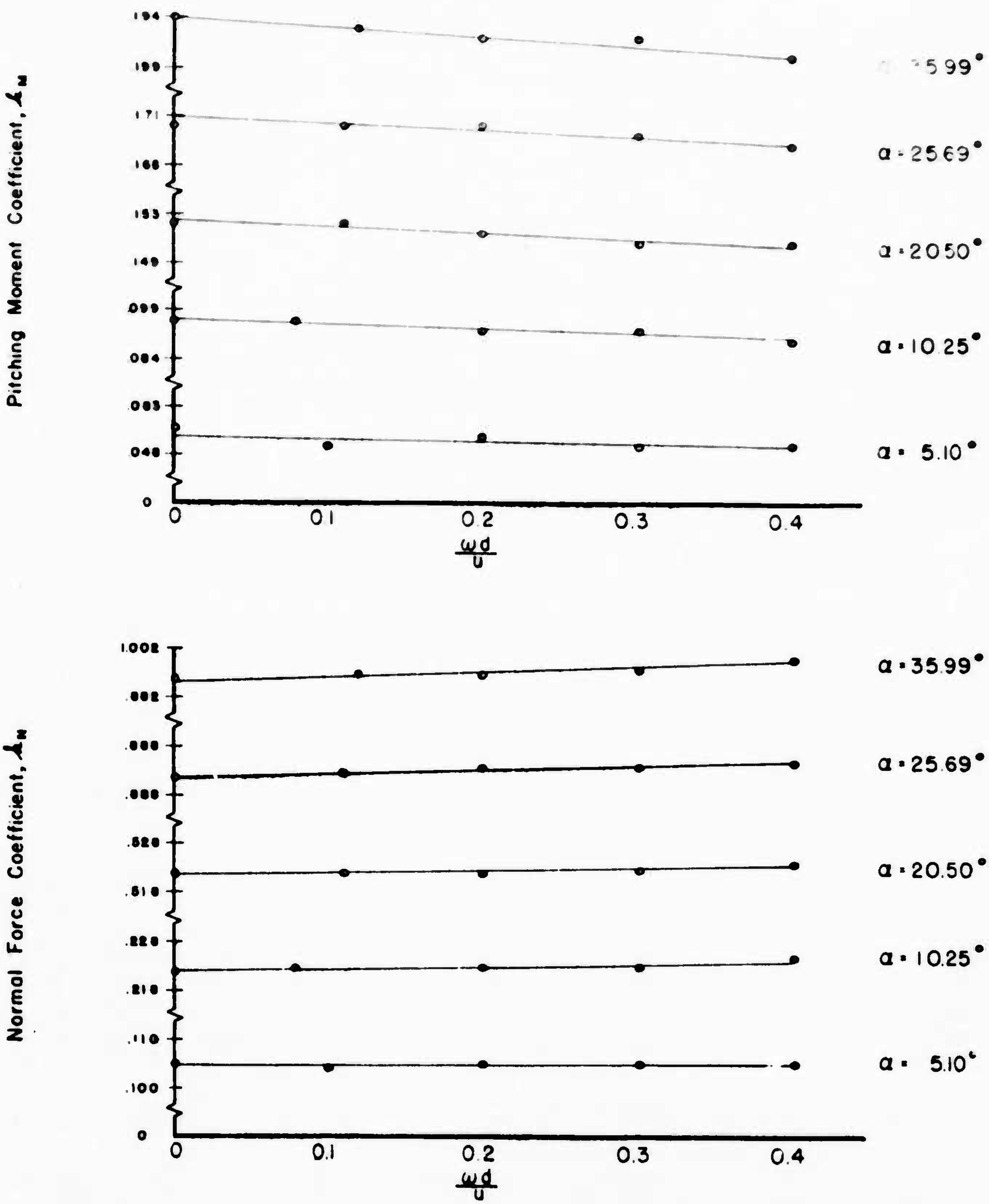

PITCH DATA VARIATION WITH SPIN FOR 30 MM BULLET

Ma = 2.00

Re = .62 x 10^6 FIG. 18

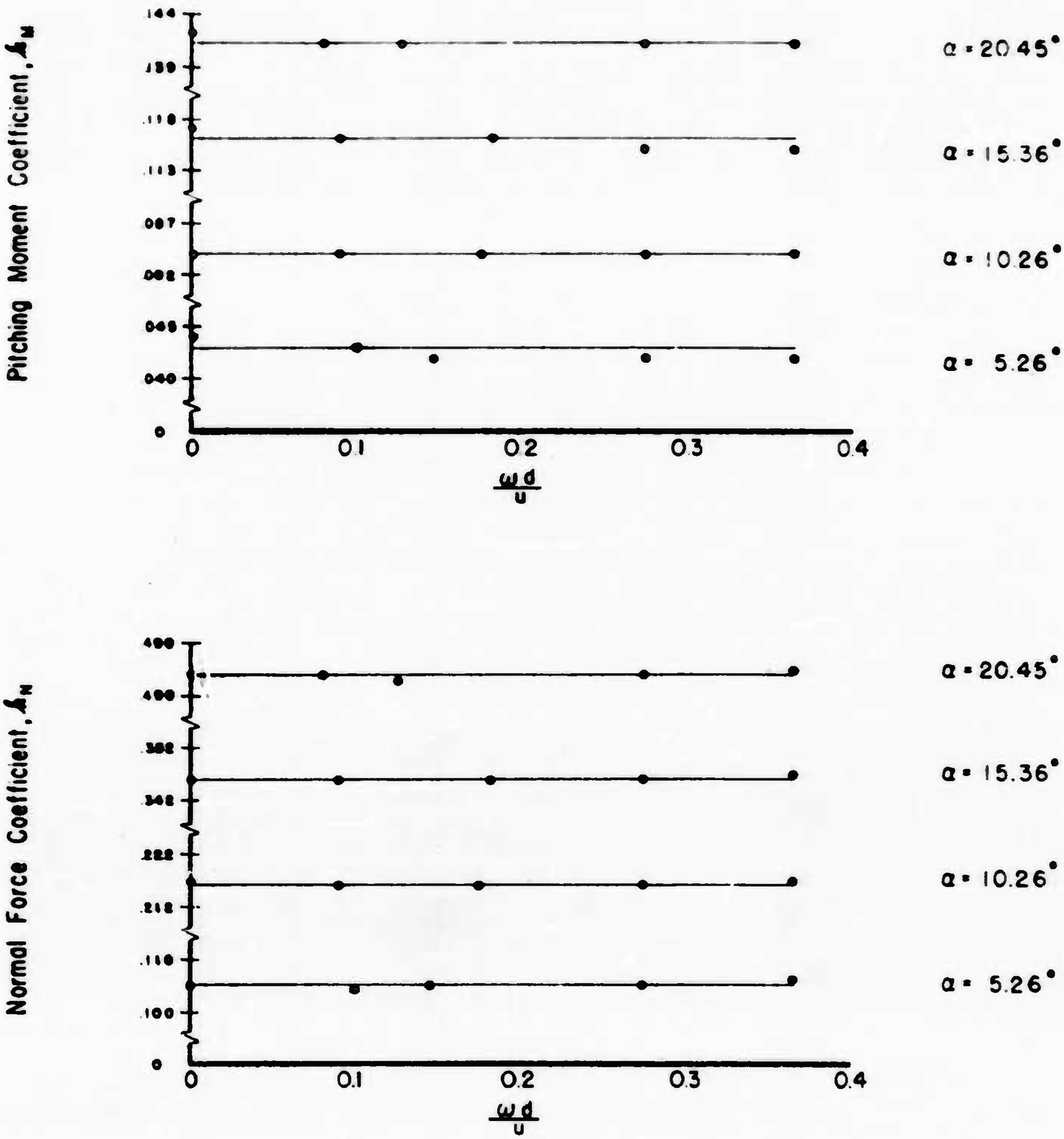

PITCH DATA VARIATION WITH SPIN FOR 30 MM BULLET

Mo = 2.47 Re = .76 x 10^6 FIG. 19

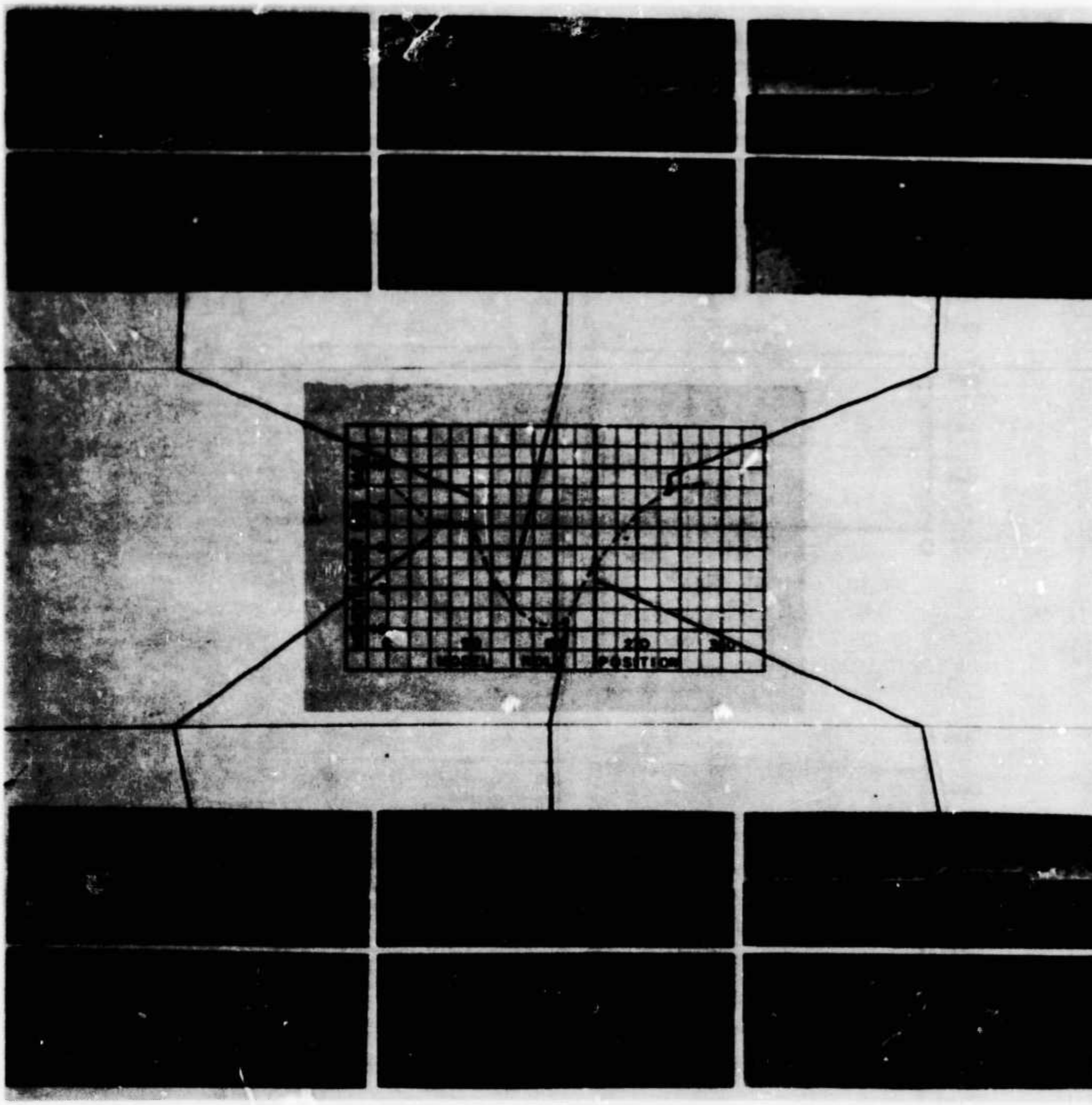

Figure 20. Illustration of Zero Shift at Re. = $.62 \times 10^6$.

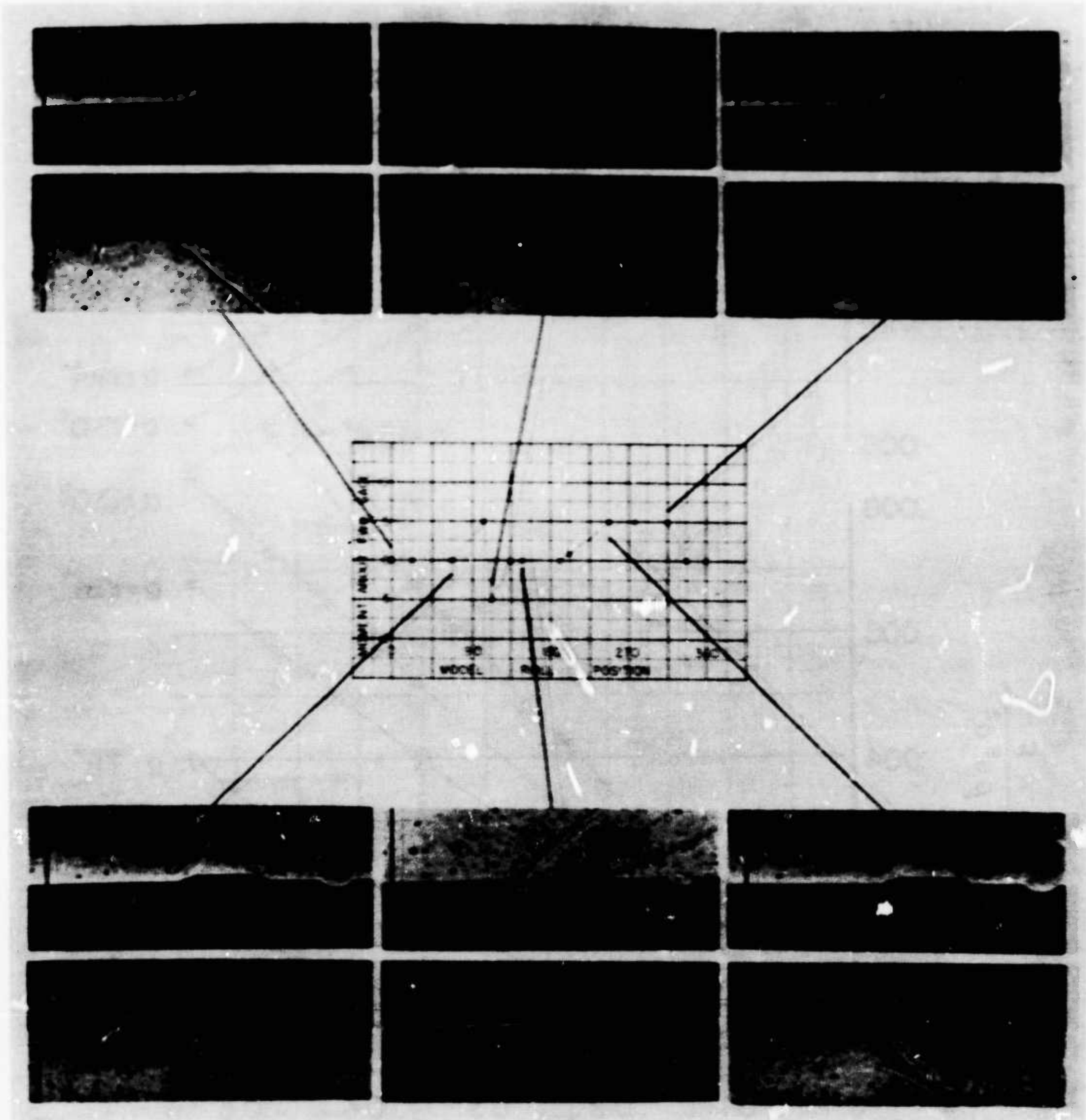

Figure 21. Illustration of Zero Shift at Re. = $.94 \times 10^6$.

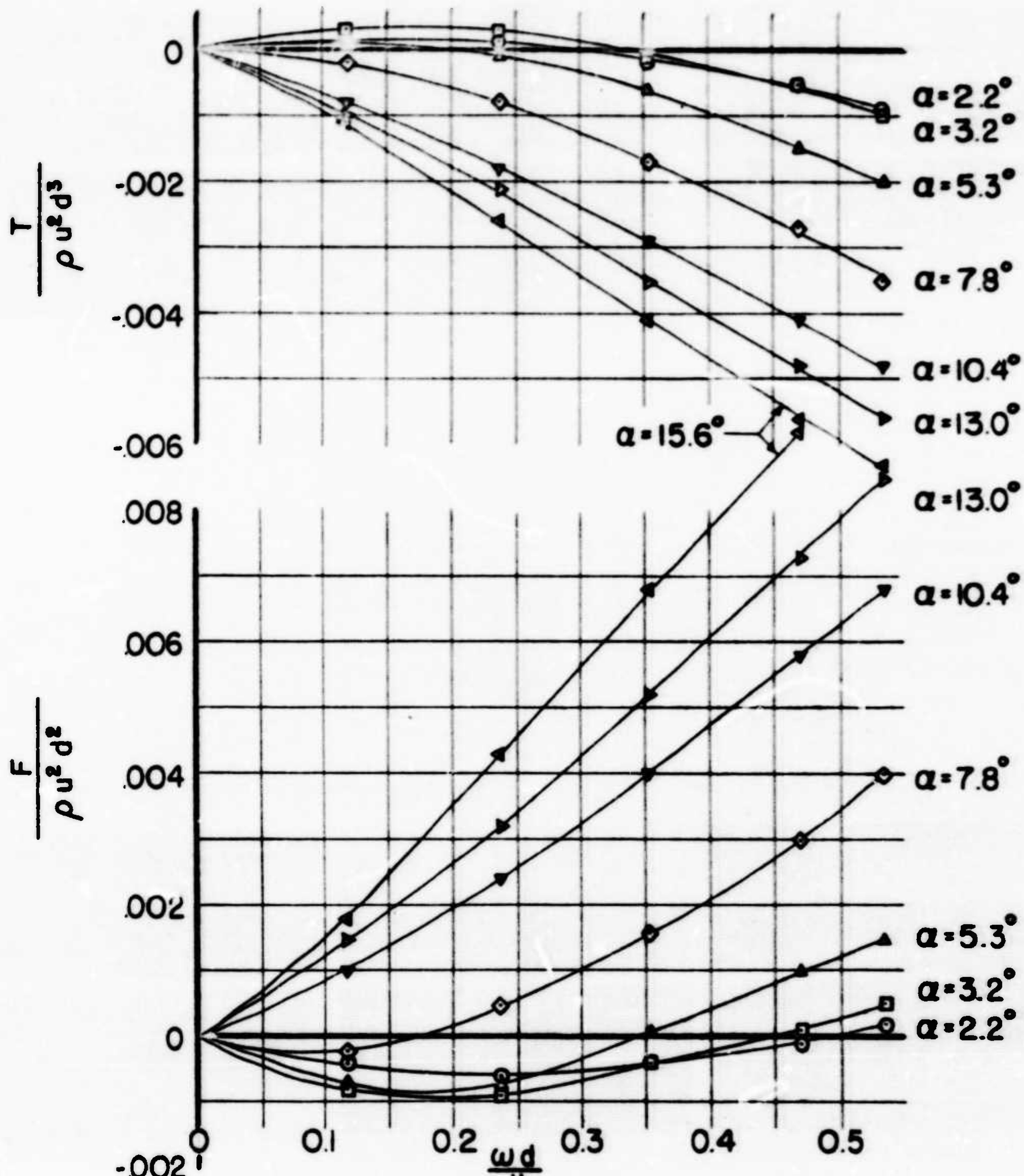

MAGNUS DATA FOR 30 MM BULLET

Ma = 1.57 FIG. 22 Re = .75 x 10^6

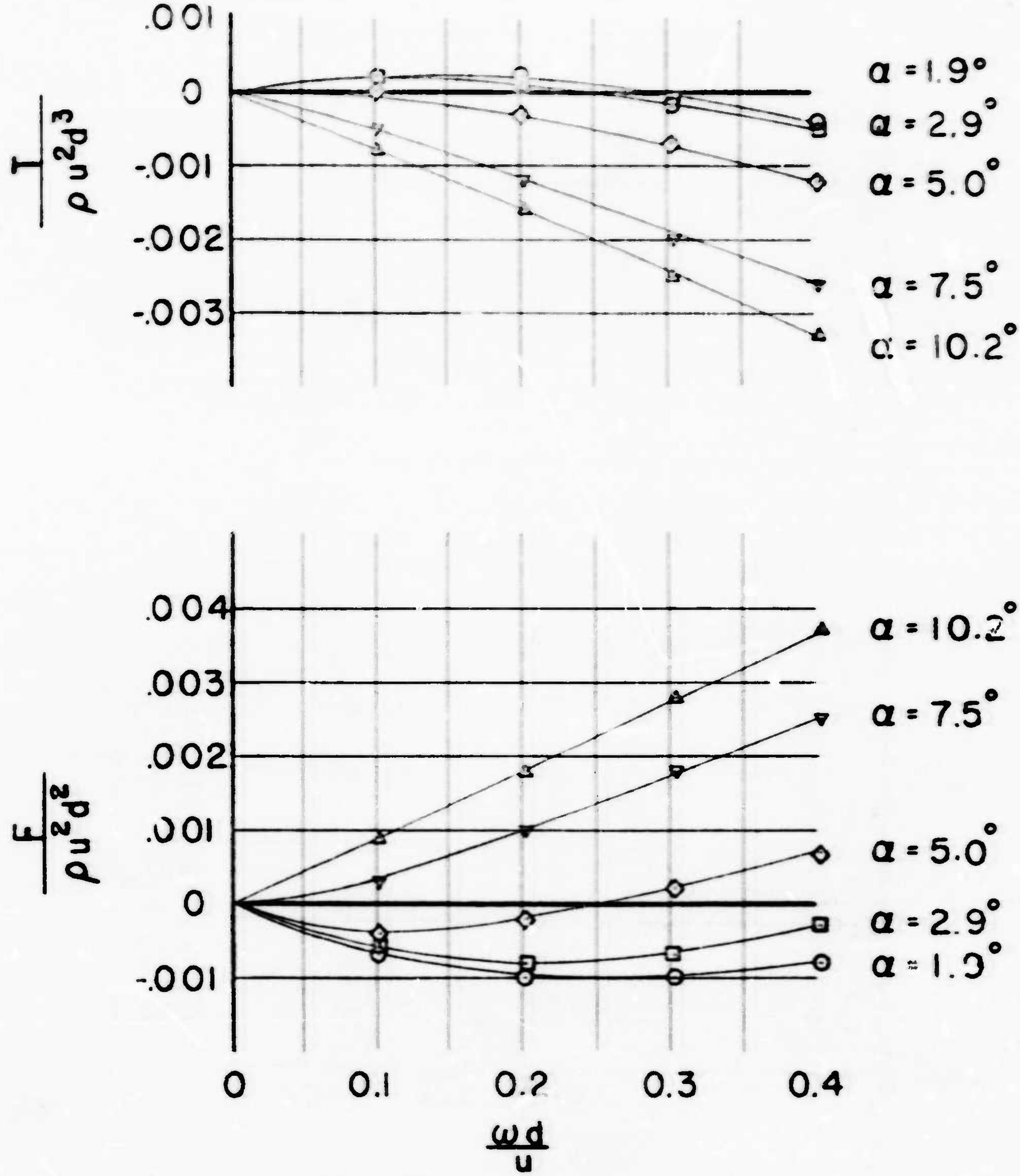

MAGNUS DATA FOR 30 MM BULLET

Ma = 2.00 FIG. 23 Re = $.94 \times 10^6$

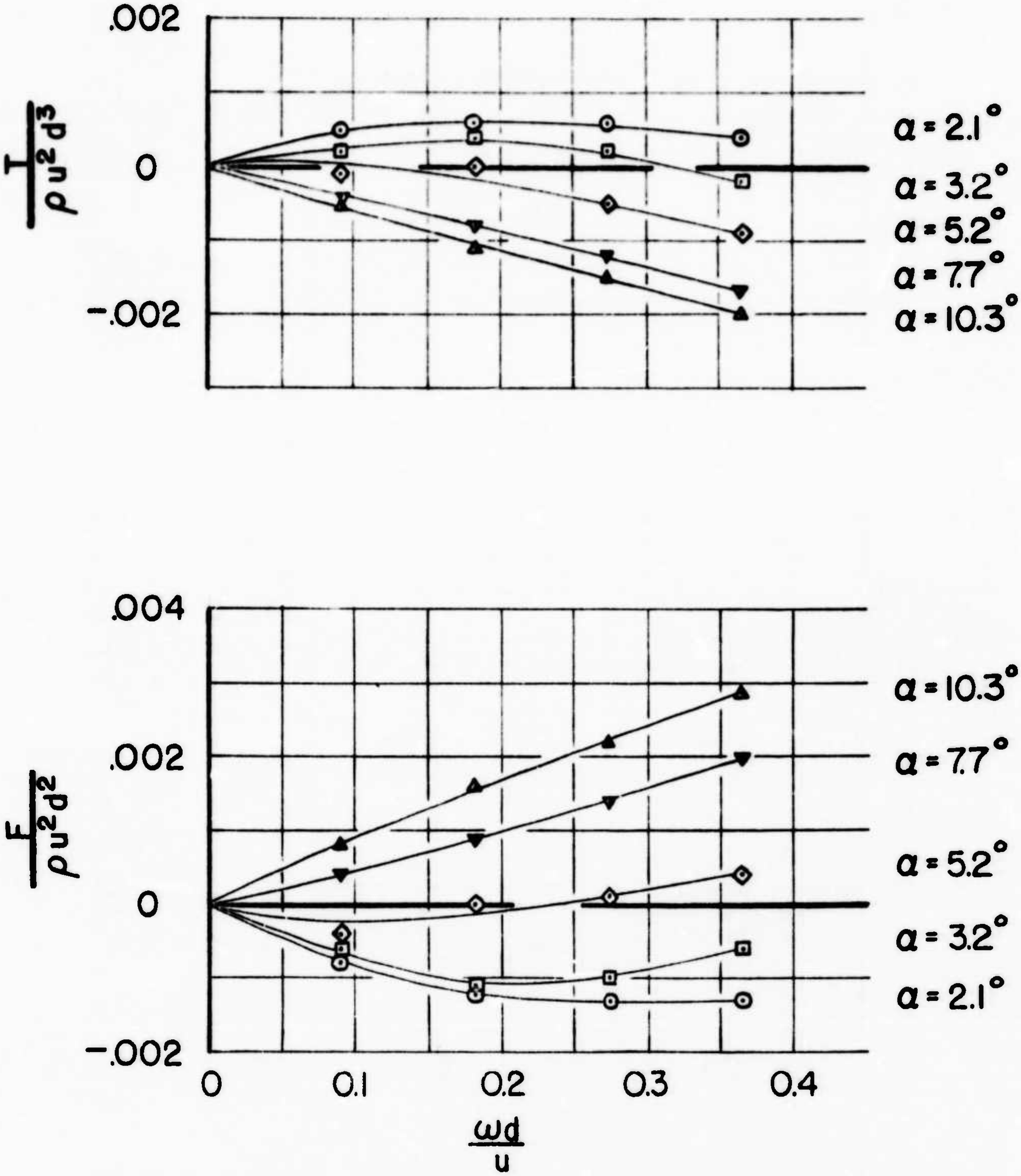

MAGNUS DATA FOR 30 MM BULLET

Ma = 2.47 FIG. 24 Re = .76 x 10^6

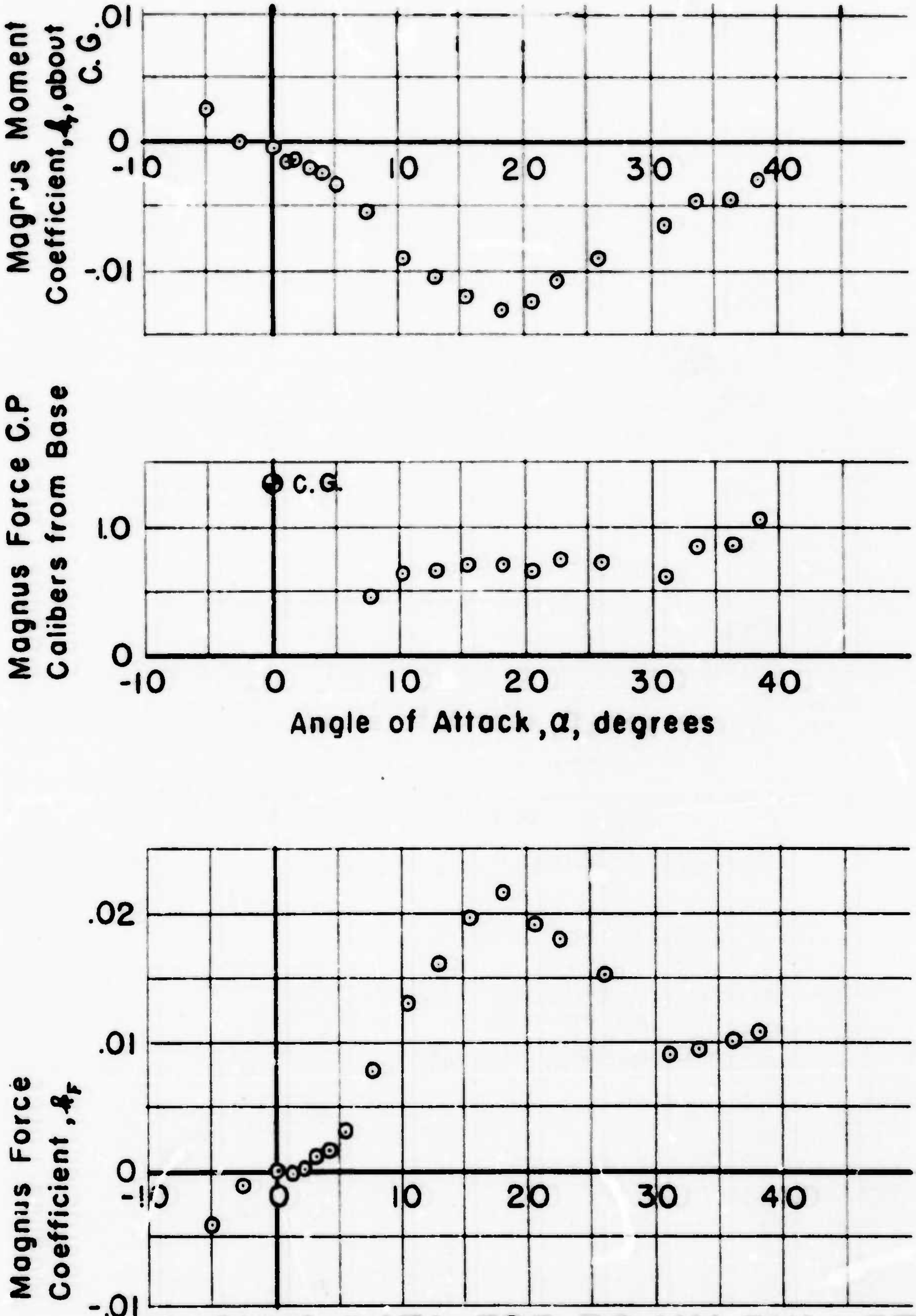

MAGNUS DATA FOR 30 MM BULLET

Ma=1.57 $\frac{\omega d}{u}$ =.536 Re=.75 x 10^6 Fig.25

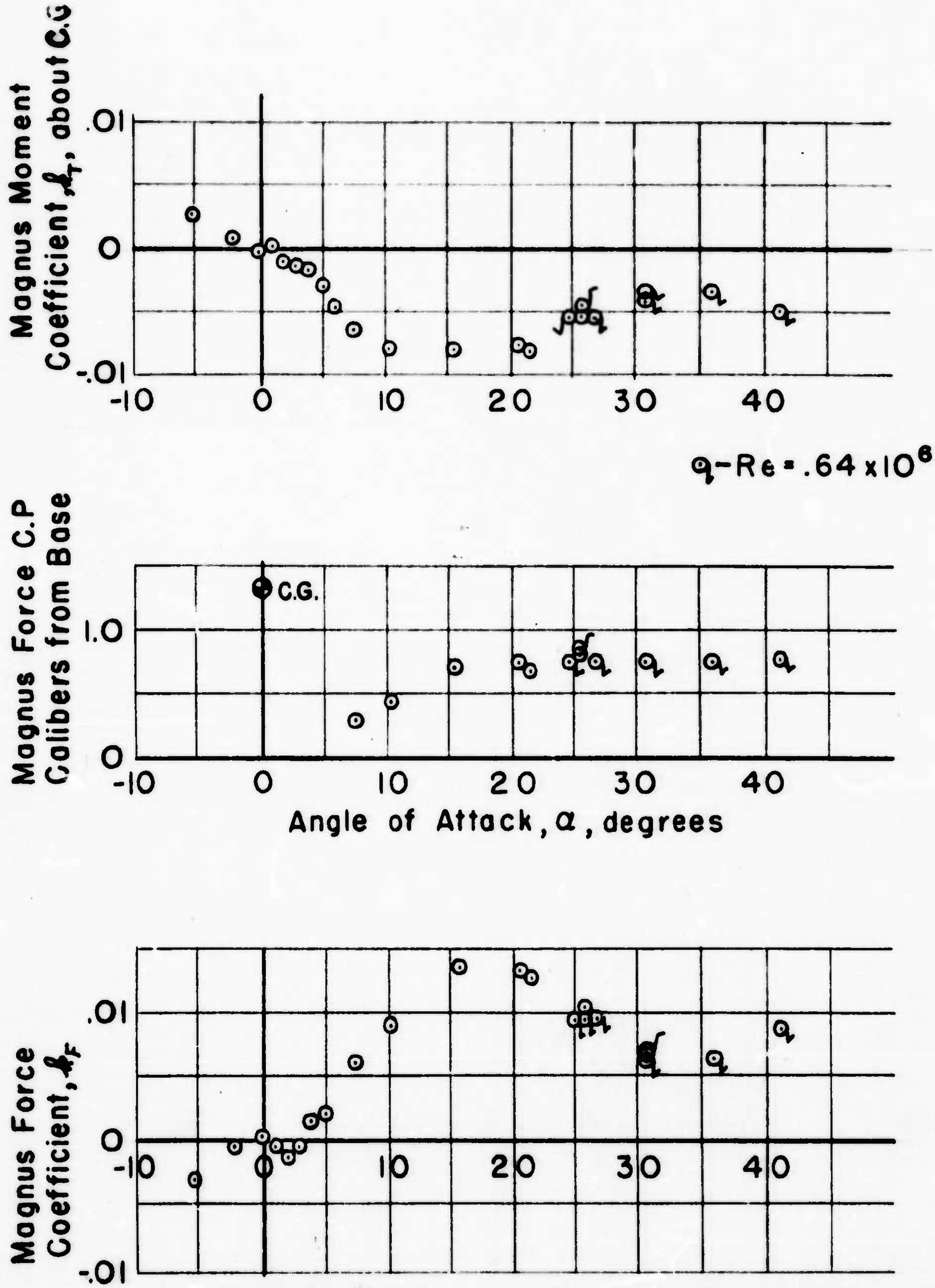

MAGNUS DATA FOR 30 MM BULLET

Ma = 2.00 $\frac{\omega d}{u}$ = 423 Re = .94 x 10^6

Fig.26

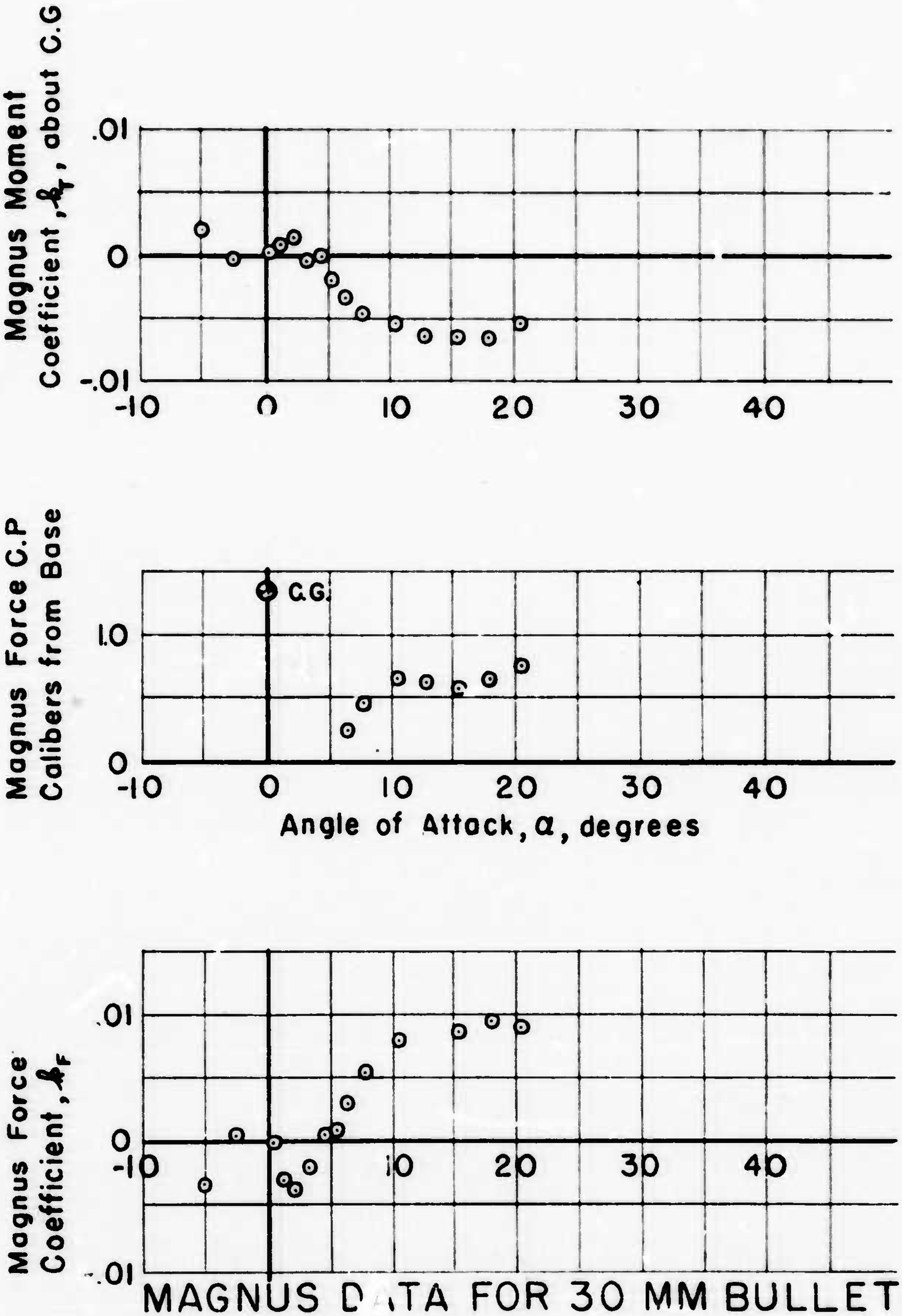

MAGNUS DATA FOR 30 MM BULLET

Ma = 2.47 $\frac{\omega d}{u}$ = .335 Re = .76 x 10^6 Fig.27

APPENDIX I

METHOD OF CALIBRATION AND DATA REDUCTION FOR A FOUR COMPONENT STRAIN GAGE BALANCE FOR MEASURING MAGNUS AND NORMAL FORCES

The aerodynamic forces and moments on the spinning model are measured using a four component strain gage balance shown in Fig. 28. The two pitch hinge lines and the two yaw hinge lines are approximately three inches apart and the front pitch and yaw hinge lines and the rear pitch and yaw hinge lines are roughly perpendicular to one another. The direction angles between the hinge lines and the normal, Magnus and axial drag directions are denoted in Fig. 28. The hinge lines are not parallel or perpendicular to one another nor in the planes of the normal, Magnus and drag forces due to unavoidable inaccuracies in centering the strain gages on the beam, to flow inclination, and misalignment of the balance in the tunnel. Hence for an accurate reduction of the data the following analysis must be made.

The moments about each hinge line produced by normal and Magnus forces can be written as

$$k_F \, m_F = N \, X_N \cos \beta_F + M.F. \, (X_M + C) \cos \gamma_F$$

$$k_R \, m_R = N \, (X_N + a) \cos \beta_R - M.F. \, (X_M + C + a) \cos \gamma_R$$

$$k_f \, m_f = N \, (X_N + C) \cos \eta_F - M.F. \, X_M \cos \epsilon_F$$

$$k_r \, m_r = N \, (X_N + C + b) \cos \eta_R + M.F. \, (X_M + b) \cos \epsilon_R$$

where

k_F, k_R, k_f, and k_r are the front pitch, rear pitch, front yaw and rear yaw gage constants respectively. m_F, m_R, m_f, m_r are the potentiometer moment readings about the front pitch, rear pitch, front yaw and rear yaw hinge lines respectively. The other symbols are defined in Fig. 28.

The distances a, b, and c; the direction angles; and the gage constants must be determined from calibration and test data before the normal and Magnus forces and their centers of pressure can be determined.

The moments about the hinge lines produced by hanging calibration weights at each of the six positions shown in Fig. 28, can be written in terms of the unknown parameters and the data recorded during the calibration (Table 1). This makes a total of 24 possible equations of which only 16 are required. Some equations will give identical results while others will give less accurate results due to small moments or the appearance of cosines of small angles. The 16 unknowns are K_F, K_R, K_f, K_r, X_n, a, b, c, β_F, β_R, γ_F, γ_R, ϵ_F, ϵ_R, η_F and η_R.

Before applying the calibration results to the wind tunnel data the calibration direction angles must be converted into the positions of the yaw and pitch hinges lines with respect to one another. This is necessary for the hinge line direction angles are dependent on the roll orientations of the balance. The relation between the hinge lines can be written as:

$$\cos \phi_F = \cos \beta_F \cos \eta_F + \cos \gamma_F \cos \epsilon_F + \cos \delta_F \cos \tau_F$$

$$\cos \phi_R = \cos \beta_R \cos \eta_R + \cos \gamma_R \cos \epsilon_R + \cos \delta_R \cos \tau_R$$

$$\cos \psi_Y = \cos \eta_F \cos \eta_R + \cos \epsilon_F \cos \epsilon_R + \cos \tau_F \cos \tau_R$$

where ϕ_F, ϕ_R, and ψ_Y are essentially the angles between the front pitch and yaw hinge lines, the rear pitch and yaw hinge lines and the front and rear yaw lines respectively.

The direction angles for the test conditions are determined from the zero spin test data at each angle of attack. For zero spin the moment equations become:

$$K_F\, m_F = NX_N \cos \beta_F$$

$$K_R\, m_R = N(X_N + a) \cos \beta_R$$

$$K_f\, m_f = N(X_N + c) \cos \eta_F$$

$$K_r\, m_r = N(X_N + c + b) \cos \eta_R$$

Here β_F, β_R, η_F, η_R are the test angles while previously the same symbols denote the corresponding calibration angles.

The hinge line relations ϕ_F, ϕ_R, and ψ_Y can also be written in terms of the test hinge line direction angles so that ten equations are available to solve for ten unknowns (eight test hinge line direction angles plus the normal force and its center of pressure).

Once the test direction angles are known, the test data obtained while the model is spinning can be inserted in the main moment equations and the equations solved for the normal, and Magnus forces and their centers of pressure.

Simplifications to the above procedure can be made which will not impair the accuracy of the results. The simplifications are: 1) The direction angles δ_Y, δ_N, τ_Y and τ_N are the same for both calibration and test. This is because the model centerline or drag centerline is rigid with respect to the balance hinge lines. 2) The change in normal force with spin is negligible so that the normal force interaction with the yaw gages is constant except for strut deflections. 3) If the direction angles ϵ_Y, ϵ_N, β_Y, and β_N are small then their cosines may be taken equal to 1 and if the angles γ_Y, γ_N, η_Y, and η_N are close to 90°, their cosines may be assumed equal to 0. In order to determine if these assumptions are valid, it is necessary to compute, for a few critical cases, the Magnus force and its center of pressure with and without the above assumption.

TABLE I

CALIBRATION EQUATIONS

For Vertical Force N_1

(1) $k_F m_F^1 = N_1 \cos \beta_F X_N$

(2) $k_R m_R^1 = N_1 \cos \beta_R (X_N + a)$

(3) $k_f m_f^1 = N_1 \cos \eta_F (X_N + c)$

(4) $k_r m_r^1 = N_1 \cos \eta_R (X_N + c + b)$

For Vertical Force N_2

(5) $k_F m_F^2 = N_2 \cos \beta_F (X_N + d)$

(6) $k_R m_R^2 = N_2 \cos \beta_R (X_N + a + d)$

(7) $k_f m_f^2 = N_2 \cos \eta_F (X_N + c + d)$

(8) $k_r m_r^2 = N_2 \cos \eta_R (X_N + c - b + d)$

For Horizontal Force $M.F._3$

(9) $k_F m_F^3 = M.F._3 \cos \gamma_F (X_N)$

(10) $k_R m_R^3 = M.F._3 \cos \gamma_R (X_N + a)$

(11) $k_f m_f^3 = M.F._3 \cos \epsilon_F (X_N + c)$

(12) $k_f m_f^3 = M.F._3 \cos \epsilon_R (X_N + c - b)$

For Horizontal Force $M.F._4$

(13) $k_F m_F^4 = M.F._4 \cos \gamma_F (X_N + d)$

(14) $k_R m_R^4 = M.F._4 \cos \gamma_R (X_N + a + d)$

(15) $k_f m_f^4 = M.F._4 \cos \epsilon_F (X_N + c + d)$

(16) $k_r m_r^4 = M.F._4 \cos \epsilon_R (X_N + c + b + d)$

For Vertical Force N_5

$$(17)\quad k_F = \xi^5_F = N_5 \left[X_N \cos a_F - P \cos b_F \right]$$

$$(18)\quad k_F = \xi^5_F = N_5 \left[(X_N - a) \cos a_F - P \cos b_F \right]$$

$$(19)\quad k_f = \xi^5_f = N_5 \left[(X_N + c) \cos a_F + P \cos b_F \right]$$

$$(20)\quad k_r = \xi^5_r = N_5 \left[(X_N + c + t) \cos a_F + P \cos b_F \right]$$

For Horizontal Force $M.F._6$

$$(21)\quad k_F = \xi^6_F = M.F._6 \left[X_N \cos a_F - M \cos b_F \right]$$

$$(22)\quad k_F = \xi^6_F = M.F._6 \left[(X_N - a) \cos a_F - M \cos b_F \right]$$

$$(23)\quad k_f = \xi^6_f = M.F._6 \left[(X_N + c) \cos a_F - M \cos b_F \right]$$

$$(24)\quad k_r = \xi^6_r = M.F._6 \left[(X_N + c + t) \cos a_F - M \cos b_F \right]$$

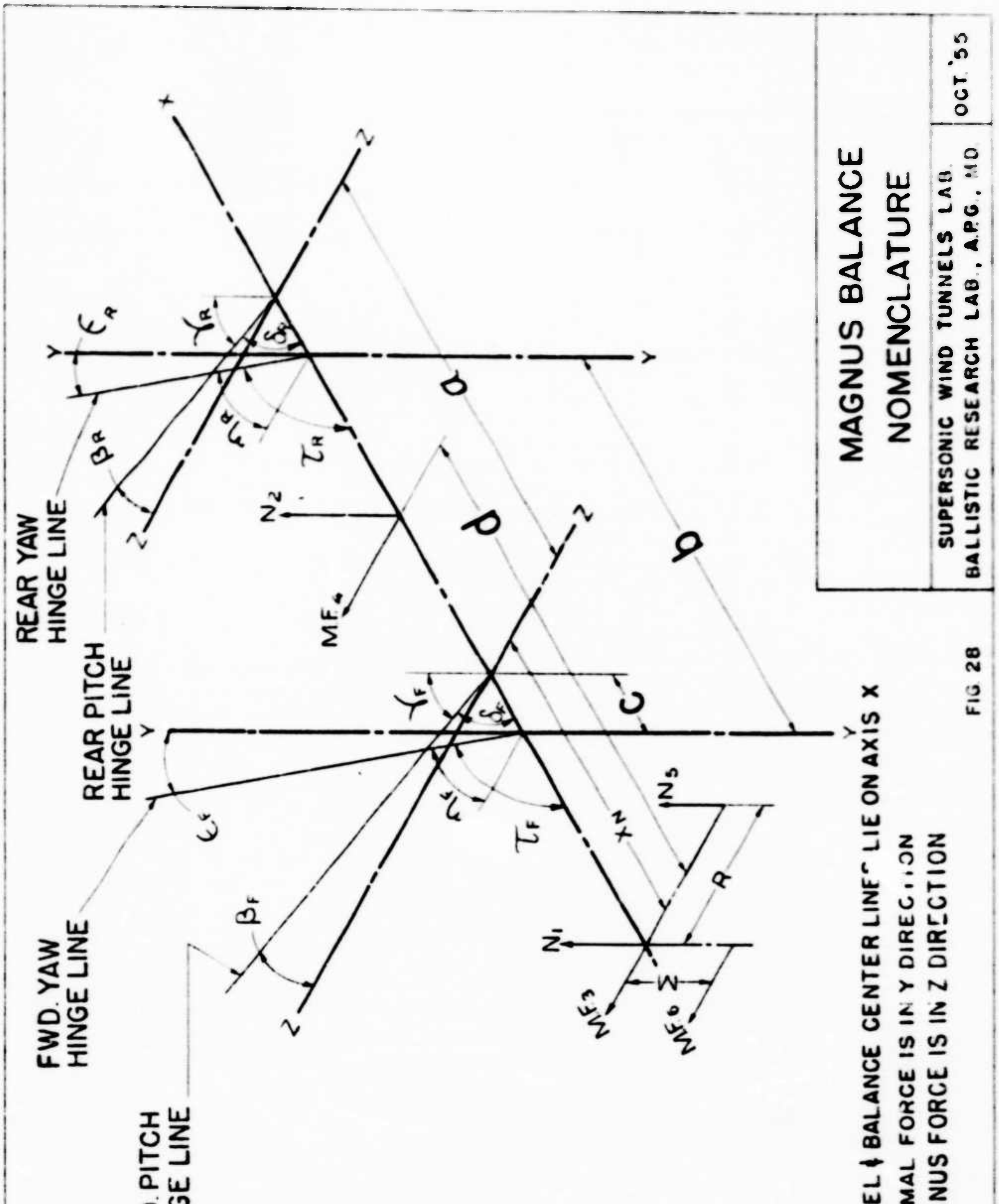
MAGNUS BALANCE
NOMENCLATURE
SUPERSONIC WIND TUNNELS LAB.
BALLISTIC RESEARCH LAB., A.P.G., MD.
OCT. '55
REAR YAW HINGE LINE
REAR PITCH HINGE LINE
FWD. YAW HINGE LINE
FWD. PITCH HINGE LINE
NOTE:
MODEL ℄ BALANCE CENTER LINES LIE ON AXIS X
NORMAL FORCE IS IN Y DIRECTION
MAGNUS FORCE IS IN Z DIRECTION

FIG 28

DISTRIBUTION LIST

No. of Copies	Organization
4	Chief of Ordnance Department of the Army Washington 25, D. C. Attn: ORDTB - Bal Sec ORDTX - AR ORDTS ORDTA
10	British Joint Ser. Mission 1800 K Street, N. W. Washington 6, D. C. Attn: Mr. John Izzard, Reports Officer
4	Canadian Army Staff 2450 Mass. Avenue Washington 8, D. C. Of Interest To: Dr. G.V.Bull CARDE
3	Chief, Bureau of Ordnance Department of the Navy Washington 25, D. C. Attn: ReO, J. D. Nicolaides
1	Superintendent Naval Postgraduate School Monterey, California
1	Commander Naval Proving Ground Dahlgren, Virginia
3	Commander Naval Ordnance Laboratory White Oak Silver Spring 19, Md. Of Interest to: Dr. Kurzweg Dr. E. Krahn Tech. Library
2	Commander Naval Ord. Test Station China Lake, California Attn: Tech. Library Dr. H. R. Kelly

No. of Copies	Organization
2	Commander Naval Air Missile Test Center Point Mugu, California
1	Commanding Officer Naval Air Dev. Center Johnsville, Pa.
1	Commanding Officer and Director David W. Taylor Model Basin Washington 7, D. C. Attn: Aerodynamics Lab.
1	Commander Air University Maxwell Air Force Base, Alabama Attn: Air Univ. Library
1	Commander Arnold Eng. Dev. Center Tullahoma, Tennessee Attn: Deputy Chief of Staff, R&D
1	Commander Air Research and Dev. Command P. O. Box 1395 Baltimore 3, Md. Attn: RDTPAG
1	Commanding General Wright Air Dev. Center Wright-Patterson Air Force Base, Ohio Attn: Mr. E. Mott WCLSW-42
4	Commander Air Force Armament Center Eglin Air Force Base, Florida Attn: ACR ACOTT ACB ACW ACRG

DISTRIBUTION LIST

No of Copies	Organization
5	Director National Advisory Committee for Aeronautics 1512 H. Street, N. W. Washington 25, D. C. Attn: Div. Research Inf.
3	Director National Advisory Committee for Aeronautics Ames Laboratory Moffett Field, California Attn: Dr. A.C. Charters Mr. H.J. Allen Mr. A. Eggers
3	Director National Advisory Committee for Aeronautics Langley Memorial Aero. Lab. Langley Field, Virginia Attn: Mr. J. Bird Mr. C.E. Brown Dr. A. Busemann
1	Director National Advisory Committee for Aeronautics Lewis Flight Propulsion Lab. Cleveland Airport Cleveland, Ohio Attn: EVAARD
2	Director, JPL Ord. Corp. Installation Department of the Army 4800 Oak Grove Drive Pasadena 3, California Attn: Mr. Irl E. Newlan, Reports Group
1	Director National Bureau of Standards Conn. Ave. and Van Ness St. N.W. Attn: G. B. Schubauer
2	U. S. Atomic Energy Comm. Sandia Corporation P.O. Box 5400 Albuquerque, New Mexico Attn: Mrs. W. K. Cox
5	Director Armed Ser. Tech. Inf. Agency Documents Ser. Center Knott Building Dayton 2, Ohio Attn: DSC - SD
1	Chief, Armed Forces Special Weapons Project P.O. Box 2610 Washington 25, D. C.
3	Commanding General Redstone Arsenal Huntsville, Alabama
3	Commanding General Picatinny Arsenal Dover, New Jersey Attn: Samuel Feltman Ammunition Labs.
2	Commanding General Frankford Arsenal Philadelphia, Pa.
1	Commanding Officer Chemical Corps Chemical and Radiological Lab. Army Chemical Center, Md.
1	Director, Operations Research Office 7100 Conn. Avenue Chevy Chase, Md. Washington 15, D. C.

DISTRIBUTION LIST

No. of Copies	Organization
2	Armour Research Foundation Ill. Institute of Tech. Technology Center Chicago 16, Illinois Attn: Mr. W.W. Casler Dr. A. Wundheiler THRU: District Chief Chicago Ord. Dist. 209 W. Jackson Blvd. Chicago 6, Illinois
1	A. D. Little, Inc. 30 Memorial Drive Cambridge 42, Massachusetts THRU: Deputy Dist. Chief Boston Ord. Dist. Boston Army Base Boston 10, Mass.
1	Aerophysics Dev. Corporation P.O. Box 657 Pacific Palisades, California Attn: Dr. William Bollay THRU: District Chief Los Angeles Ord. Dist. 55 S. Grand Avenue Pasadena 2, California
1	ARO, Inc. Tullahoma, Tennessee Attn: Mr. R. Smelt THRU: Deputy Dist. Chief Cincinnati Ord. Dist. Big Four Building Cincinnati 2, Ohio
2	Applied Physics Laboratory 8621 Georgia Avenue Silver Spring, Maryland THRU: Naval Inspector of Ord. Applied Physics Lab. Johns Hopkins University 8621 Georgia Avenue Silver Spring, Md.
1	Cornell University Graduate School of Aero. Ithica, New York THRU: National Advisory Committee for Aeronautics 1512 H Street, N.W. Wash. 25, D. C.
2	Cornell Aero. Lab., Inc. Buffalo, New York Attn: Miss Elma T. Evans, Librarian Of Interest to: Mr. W.S. Young THRU: Bureau of Aero. Representative Cornell Aero. Lab., Inc. P.O. Box 235 Buffalo 21, New York
1	CONVAIR Div. of General Dynamics Corp. Ord. Aerophysics Lab. Daingerfield, Texas Attn: Mr. J.E. Arnold THRU: Asst. Inspector of Naval Material Ord. Aerophysics Lab. Daingerfield, Texas
1	Firestone Tire and Rubber Company Defense Research Div. Akron 17, Ohio Attn: Peter J. Ginge THRU: Deputy Dist. Chief Cleveland Ord. Dist. Lincoln Bldg. 1367 E. 6th St. Cleveland 14, Ohio

DISTRIBUTION LIST

No. of Copies	Organization
1	Guggenheim Aero. Lab. California Inst. of Tech. Pasadena 4, Calif. Attn: Professor H.W. Liepman THRU: District Chief Los Angeles Ord. Dist. 55 S. Grand Avenue Pasadena 2, Calif.
1	General Electric Company Library, GM Department 2900 Campbell Avenue Schenectady 6, New York Attn: Jack M. McCormick THRU: Air Force Plant Rep. General Electric Co. 1 River Road Schenectady, New York
1	M. W. Kellogg Company Foot of Danforth Avenue Jersey City 3, New Jersey Attn: Miss E.M. Hedley THRU: Inspector of Naval Material Naval Industrial Reserve Shipyard Building 24, Port Newark Newark 5, New Jersey
2	Mass. Institute of Technology Instrumentation Lab. 155 Mass. Avenue Cambridge 39, Mass. Attn: Dr. C.S. Draper THRU: Inspector of Naval Material Mass. Institute of Tech. Cambridge 39, Mass. Attn: Dev. Contract Dept.
1	North Carolina State College Raleigh, North Carolina Attn: Prof. J. W. Cell THRU: Deputy Dist. Chief Philadelphia Ord. Dist. 128 North Broad St. Philadelphia 2, Pa.
1	Princeton University Aero. Department Princeton, New Jersey Attn: Prof. Wallace Hayes THRU: National Advisory Committee for Aeronautics 1512 H Street, N.W. Wash. 25, D. C.
2	United Aircraft Corp. Research Dept. East Hartford 8, Conn. Attn: Mr. Robert C. Sale Mr. M. Schweiger THRU: Bureau of Aero. Representative Pratt and Whitney Aircraft Div. United Aircraft Corp. East Hartford 8, Conn.
1	Univ. of Southern Calif. Engineering Center Los Angeles 7, Calif. Attn: Mr. H.R. Saffell, Director THRU: Bureau of Aero. Rep. Aerojet Eng. Corp. 6352 N. Irvindale Ave. Azusa, Calif.

DISTRIBUTION LIST

No. of Copies	Organization	No. of Copies	Organization
1	University of Michigan Willow Run Research Center Willow Run Airport Ypsilanti, Michigan Attn: Mr. J.E. Corey THRU: Commander Central Air Procurement District West Warren and Lonyo Avenues Detroit 32, Michigan	1	Professor H.W. Emmons Harvard University Cambridge 38, Mass.
		1	Dr. Clark B. Millikan Calif. Instit. of Tech. Pasadena, Calif.
		1	Dr. A.E. Puckett Hughes Aircraft Co. Florence Ave. at Teal St. Culver City, Calif.
1	Wright Aero. Corporation Wood-Ridge, New Jersey Attn: Sales Dept (Government) THRU: Air Force Plant Rep. Wright Aero. Corporation Wood-Ridge, New Jersey	1	Dr. L.H. Thomas Watson Scientific Computing Lab. 612 West 116th Street New York 27, New York
		1	Naval Supersonic Lab. Mass. Institute of Tech. Cambridge 39, Mass. Attn: Mr. Frank H. Durgin
1	Professor George Carrier Div. of Applied Sciences Harvard University Cambridge 38, Mass.	1	Office, Assistant Secretary of Defense (R&D) Committee on Ordnance Washington 25, D. C.